DEVELOPMENT OF FUNDAMENTAL UNDERSTANDING OF THE CURE KINETICS OF BENZOXAZINE EPOXY BLENDS

A Thesis
Presented to
The Academic Faculty

By

Adam Maffe

In Partial Fulfillment
Of the Requirements for the Degree
Master of Science in Materials Science and Engineering

Georgia Institute of Technology

May, 2020

DEVELOPMENT OF FUNDAMENTAL UNDERSTANDING OF THE CURE KINETICS OF BENZOXAZINE EPOXY BLENDS

Approved by:

Dr. Satish Kumar, Advisor
School of Materials Science and Engineering
Georgia Institute of Technology

Dr. Meisha Shofner
School of Materials Science and Engineering
Georgia Institute of Technology

Dr. Dhriti Nepal
Air Force Research Laboratory

Date Approved: January 6th, 2020

ACKNOWLEDGEMENTS

I would like to thank my parents and brother and for their continuous support throughout my entire graduate school career, whether it be at Georgia Tech or at AFRL in Ohio. I would not have been able to complete this endeavor without them.

I also express my most sincere gratitude to my advisor at Georgia Tech, Dr. Satish Kumar for guiding me along the tumultuous path of identifying a project and providing funding for my research. Thanks should also go to Dr. Donggang Yao for initially accepting me into the Georgia Tech MSE graduate program. Additionally, this project would not have been able to be completed without the guidance and funding provided by Dr. Dhriti Nepal at AFRL and from the Southern Ohio Council for Higher Education (SOCHE). I would also like to thank Dr. Shofner for taking the time and consideration to be a part of my defense committee.

I owe gratitude to the students I worked alongside in Dr. Kumar's group, Dr. Yao's group and my coworkers at AFRL. Special thanks to Jeff Luo, for acting as a catalyst for my move to Dr. Kumar's group.

I am extremely grateful and appreciative for the post-doc in my group at AFRL, Spencer Hawkins. His daily suggestions and company in the lab made this experience enjoyable and helped me to not only grow in a scientific sense, but also as a person.

Finally, thank you to all Georgia Tech and AFRL staff that helped to train me on equipment and facilitated the completion of this research.

TABLE OF CONTENTS

LIST OF TABLES

LIST OF FIGURES

LIST OF SYMBOLS AND ABBREVIATIONS

A: Absorption

A: Pre-Exponential Factor

Bz: Benzoxazine

c: concentration

CER: Cycloaliphatic Di-Functional Epoxy Resin

cP: centipoise

DGEBA: Diglycidyl Ether of Bisphenol A

DSC: Differential Scanning Calorimetry

DMA: Dynamic Mechanical Analysis

E_a: Activation Energy

f(α): phenomenological model

FT-IR: Fourier Transform Infrared Spectroscopy

G′: Shear Storage Modulus

G″: Shear Loss Modulus

H_T: Heat of Reaction

K(T): Temperature Dependent Rate Constant

l: Path Length

M_c: Distance between crosslinks

MIR: Mid-IR

NIR: Near-IR

NMR: Nuclear Magnetic Resonance

R: Universal Gas Constant

T_g: Glass Transition Temperature

TGAP: Triglycidyl para-aminophenol Epoxy Resin

TGGDM: Tetraglycidyl-4,4”-diaminodiphenylmethane

T_P: Peak Temperature

α: Degree of Conversion

β: Heating Rate

ΔH: Change in Enthalpy

ε: Molar Absorptivity Coefficient

ν: Crosslink Density (mol/m^3)

ρ: Bulk Density

Φ: Heat Flow

SUMMARY

This study attempts to bridge the gap between the current fundamental understanding of benzoxazines on the monomer level and their macro scale thermo-mechanical properties. Bisphenol-A based benzoxazine (Bz) was blended with di- and tri-functional epoxies to reduce viscosity for processing, and their resulting thermal and mechanical properties were characterized. Additionally, the formation of inter-molecular and intra-molecular hydrogen bonds was investigated within a Bz-epoxy two component system. Activation energy, heat of reaction, degradation temperature, hydrogen bonding characterization and thermo-mechanical characterization were studied using a differential scanning calorimeter, dynamic mechanical analyzer, thermogravimetric analysis, Fourier transform infrared spectroscopy and quasistatic tensile testing. Preliminary results show a synergistic increase in T_g of the blends, for both di- and tri-funcitonal epoxy blends. Surprisingly, while the two components exhibit T_g's of ~ 150-170 ^oC, the blended systems consistently exhibited a T_g in the range of 210-250 ^oC. This work aims to expand upon thermal and mechanical characterization data generated by our collaborator Ehsan Barjasteh for the benzoxazine – di-functional epoxy system, as well as explore a new benzoxazine – tri-functional epoxy-based system. Our underlying motivations in this study are to identify the origins of the synergistic increase in T_g upon blending through various thermo-mechanical characterization methods and in-situ FT-IR analysis of cure kinetics, as well as identifying the compositions and functionality which exhibit the most desirable combination of thermal and mechanical properties.

CHAPTER 1

INTRODUCTION

Thermoset polymers have been extensively used for applications including those demanding extreme thermo-mechanical performance as well as resistance to extreme environments. Generally, thermoset systems consist of two to three components including: a base resin, hardener and optionally a catalyst. Catalysts can be added to accelerate the curing process. Unlike thermoplastic polymers, thermoset polymers are required to be cured in order to form an infinite 3D network of crosslinks. In many thermoset systems, the base resin and hardener react to form irreversible covalent bonds known as crosslinks. As a result of the tightly formed crosslinked network, thermoset polymers often exhibit desirable properties such as high strength, low shrinkage, chemical resistance and relatively high temperature resistance. However, thermosets tend to lack toughness, are susceptible to moisture and cannot be reprocessed [1].

Common thermoset polymers include polyester, epoxy, bismaleimide, cyanate ester, polyimides and phenolics. Polyesters are widely used in commercial applications due to their relatively low production cost. They tend to exhibit lower thermo-mechanical properties, lower water resistance and notable cure shrinkage relative to more performance grade thermosets. Polyesters may also be formulated to cure at room temperature or elevated temperatures depending on the processing technique desired and final application requirements. Vinyl esters are a subset of polyesters which only contain reactive ester groups at the ends of the monomer. This yields a higher toughness than most other polyesters but is accompanied by a lower crosslink density.

Polyimides were developed for use in high temperature applications ranging from 260 – 315 ^{o}C. Crosslinking of the network proceeds via condensation or addition polymerization. Management of volatiles is crucial in processing polyimides if the reaction proceeds via condensation. Unfortunately, polyimides require significantly higher temperature and pressures to process relative to epoxies, so existing processing methods must be modified [2].

Bismaleimide resins fill the gap in thermo-mechanical performance between polyimides and epoxies. BMI's exhibit T_g in the range of 220-315 ^{o}C. They require elevated temperature cure cycles (~175 ^{o}C) and are often subjected to a higher temperature post cure stage (~230 ^{o}C). Early BMI material proved difficult to process, however, the field of research has matured enough to allow use in already existing processing methods. The primary downfall of BMI's is their susceptibility to "imide corrosion" in saltwater environments. Imide corrosion is a type of hydrolysis which degrades the BMI [3].

Cyanate esters exhibit T_g within the range of 190-290 ^{o}C, due to their high aromatic ring content. Cure proceeds as oxygen linked triazine rings and bisphenol units crosslink [4]. Cyanate esters are often used in applications which require a low dielectric constant such as antennas. Cyanate esters are not as commonly used as other thermosets due to their high cost.

Epoxy resins are the most common type of thermoset polymer used in composite and adhesive applications. In addition to their high strength and low cure shrinkage, large processing windows can be achieved through blending epoxies and altering their cure profiles. Crosslinking of epoxy resins occurs at the oxirane location in the monomer. The oxirane ring is generally present in the form of a glycidyl amine, glycidyl ether or aliphatic

ring. Glycidyl type epoxies tend to be used for composite applications while cycloaliphatic type epoxies are used as a minor epoxy component in thermoset blends to control viscosity during processing [5].

The two most common epoxies used in the industry are diglyciyl ether of Bisphenol A (DGEBA) and tetraglycidyl-4,4”-diaminodiphenylmethane (TGGDM). TGGDM has more epoxy groups per monomer than DGEBA, leading to a more densely crosslinked network with increased mechanical properties. The primary downfall of increased crosslink density is increased brittleness of the final product.

Aliphatic amines and aromatic amines can be used as curing agents for epoxy resin systems. Aliphatic amines are much more reactive and are therefore suitable for cure at room temperature. Aromatic amines require elevated temperature for cure, but yield improved mechanical properties and lower cure shrinkage than systems using aliphatic amines as a curing agent [5].

Phenolic resins are desirable due to their low flammability, low smoke production and ablative resistance. Because of these properties, phenolics are often used in aircraft interiors and as heat shields in high temperature applications.

Polybenzoxazines (PBz) are a relatively new phenolic-type thermoset which possess desirable properties including high thermo-mechanical properties, high chemical resistance, low moisture absorption, low CTE and no volatile release during cure [6-11]. A relative comparison of thermo-mechanical properties as well as cure characteristics with other common thermosetting resins is shown in Table 1. The three main components required for benzoxazine synthesis are a phenol, amine and formaldehyde. Synthesis occurs via Mannich condensation [12]. Due to the ease of synthesis, benzoxazine monomers can

be tailored to contain various functional groups. One common example is including long aliphatic chains in the backbone of the benzoxazine monomer to increase flexibility and strain at failure.

Table 1: Qualitative review of common thermosets and their properties. Adapted from [13].

Property	Benzoxazine	Epoxy	Phenolic	BMIs
T_g	Good	Good	Good	Excellent
Stiffness	Excellent	Good	Good	Good
Toughness	Average	Good	Average	Average
Shrinkage	Excellent	Poor	Good	Good
Flammability	Excellent	Poor	Excellent	Good
Chemical Resistance	Excellent	Average	Good	Good
CTE	Good	Average	Average	Good
Processability	Good	Good	Poor	Average

Although extensive studies on the variety of Bz monomer synthesis have been performed, little work has been conducted on relating bulk scale properties to the chemical structure of the crosslinked network. The incorporation of benzoxazine into current manufacturing practices requires a melt viscosity within the range of 100-1000 cP. Benzoxazine exhibits a relatively high melt viscosity (>1250 cP) [14] within common processing window (80-110 ^{o}C). This inherently high viscosity can cause problems in composite manufacturing, failing to wet out fiber tows and resulting in voids and structural

defects. High viscosity also makes incorporation of the polymer into already existing processing techniques difficult. Additionally, single component homopolymerized PBz exhibits a glass transition (T_g) of roughly 150 ^oC, which is significantly lower than aerospace grade epoxies. Benzoxazines are far from a mature field of study, with significant challenges remaining such as lowering processing viscosity and increasing thermo-mechanical properties. Because of these difficulties, benzoxazines are not commonly used in commercial applications. Figure 1 depicts an overview of the current availability of thermoset materials with their relative thermal performance vs. cost.

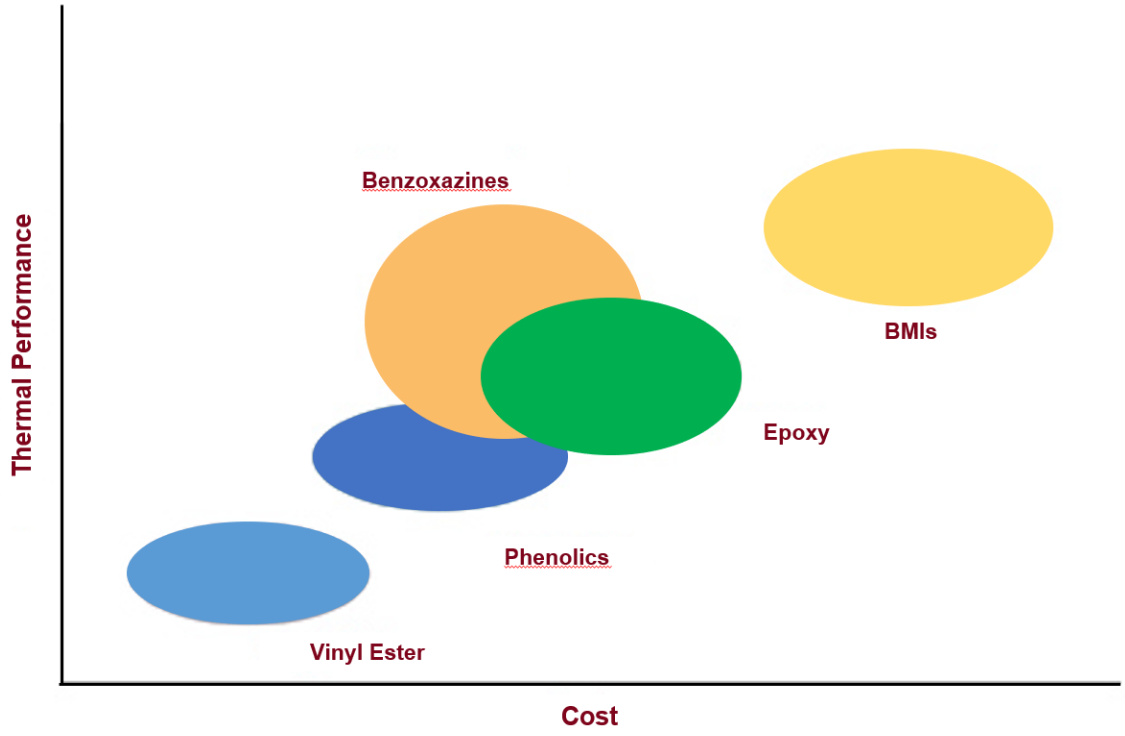

Figure 1: Thermal performance vs. cost of common thermoset materials. Adapted from reference [13].

Studies conducted by Ishida and Allen have shown great promise for developing hybrid networks with benzoxazine-epoxy blend systems, both lowering the processing viscosity and increasing final thermal properties such as T_g [15]. A study performed by

Barjasteh et. al. [14] have showed that varying the content of epoxy with benzoxazine significantly altered the T_g of the cured network. It is also known that the functionality of the alloyed epoxy will affect the final crosslink density, and likely the thermo-mechanical properties. This thesis focuses on identifying the Bz/Ep ratio and epoxy functionality which yield the most desirable combination of final thermo-mechanical properties post-cure. Various thermal, mechanical and spectroscopic techniques are utilized to characterize hybrid network formation during cure and bulk scale properties.

CHAPTER 2

LITERATURE REVIEW AND OBJECTIVES

2.1 Introduction

Thermoset use in the construction, automotive and aerospace industries has increased in recent years. Adaptation of a new resin into these industries requires broadening of the resin processing window. Neat Bz is solid at room temperature and cannot readily be processed using existing techniques. The processing window can be expanded through controlled experimentation and characterization of Bz-epoxy resin blends and their viscosities. Epoxy weight percent as well as epoxy functionality can be varied to control the end properties of these hybrid network Bz/Ep cured systems. Blending Bz with epoxy will require identification of an optimal cure cycle to ensure maximum degree of cure is reached while avoiding degradation. Altering the functionality of the epoxy will also require significant changes in the cure cycle. Quantification of the bulk scale properties and cure kinetics can be achieved through utilization of differential scanning calorimetry, dynamic mechanical analysis and Fourier transform infrared spectroscopy

2.2 Benzoxazine Resin

The Bz group of resins was designed to combine the mechanical properties of epoxy and the thermal and flame retardance properties of phenolics. Bz presents many desirable properties such as low cure shrinkage, ability to form hydrogen bonds, no volatile production during cure and high flammability resistance [16].

Although Bz presents many desirable properties, it is difficult to process, requirinh higher curing temperatures and is brittle post cure. Additionally, homopolymerized Bz systems have been shown to exhibit a significantly lower crosslink density compared to other thermoset resin systems while maintaining comparable thermo-mechanical properties. This is likely due to the dense hydrogen bonding that readily forms in Bz networks [17].

2.3 Benzoxazine-Epoxy Hybrid Systems

Blending Bz and epoxy is an attractive route to improve processing windows as well as post-cure thermo-mechanical properties. Although Bz resin presents many desirable properties such as high T_g, low cure shrinkage, and no volatile release upon cure, it does have several notable shortcomings. These include being solid at room temperature, inability to process within existing industrial processing windows and its high rigidity post cure. Blending Bz resin with epoxy presents a solution to both undesirable characteristics.

Epoxy resins have long been used in many industries, with some of their most prominent use being in the fields of coatings and adhesives. Generally epoxy resin exhibits good chemical resistance and acceptable mechanical strength, while its final properties are primarily dictated by which hardener is used in the system. The four classes of hardeners that are widely used are amine compounds, acid anhydrides, Lewis acids and polyamides group. Each curing agent imparts a unique property to the system. For example, amine-based curing agents are toxic but allow the curing reaction to proceed at room temperature.

Rimdusit et. al. tested arylamine based Bz resins as a curing agent for a bisphenol-a based epoxy system and observed an higher temperature processing range and a

synergistic increase in the T_g at the optimal Bz/Ep mass ratio of 80:20. It was also reported that flexural strength and flexural strain at break increased with increasing epoxy content, while flexural modulus decreased [18].

A similar study by Ishida and Allen proposed that the crosslink density within Bz networks could be increased through inclusion of epoxy, specifically DGEBA. As the ring opening polymerization of Bz proceeds, phenolic groups are produced, allowing epoxide groups to readily crosslink into the network. Ishida proposed that the theoretical crosslink density of the alloyed hybrid network would increase, due to an increase in the number of available reactive sites at which crosslinks could form. The highest T_g observed in the study was 156 ^oC, obtained from the system containing 30 mol % epoxy. As increasing amounts of epoxy, beyond 45 mol %, were added to the system the thermo-mechanical properties declined sharply. Ishida and Allen proposed that in the case of excess epoxy, the phenolic groups generated by the oxazine ring opening not only participated in the reaction, but also served to catalyze the reaction. They observed lower molecular weight oligomers which were noted to act as plasticizers in the network. Results from the study corroborated their hypothesis that crosslink density increased with increased mol % of epoxy. T_g was found to increase with added epoxy, but decreased at and above 45 mol% epoxy. Flexural modulus decreased upon the addition of any epoxy, while flexural strength and flexural strain to failure increased [15].

In order to deal with the inherent brittleness of Bz, Rimdusit et. al. alloyed bisphenol-A based Bz with a flexible epoxy and elastomeric urethane. Through FT-IR analysis, Rimdusit et. al. were able to confirm that a hybrid network formed in both cases; alloying of Bz/Ep and alloying of Bz/Urethane. Alloy's containing 10 wt% or less urethane,

or 30 wt% or less epoxy were found to have improved flexural strength compared to the neat Bz system. T_g's were found to increase with increasing levels of urethane, while decreased with increasing levels of epoxy [19]. Alloys of bisphenol-F Bz and bisphenol-F novolac resins with intercalated aliphatic segments were also investigated by Kumar and Nair in an attempt to improve the flexibility, and toughen bisphenol-F Bz [20].

A proper cure profile is crucial to achieve the desired post-cure final thermo-mechanical properties. Identification of a proper cure profile also allows control over the network structure as well as tailoring of the final crosslink density [21]. Improper cure profiles can lead to smaller molecular weight molecules within the final infinite 3-dimensional network, causing detrimental effects such as plasticization. Off stoichiometric blends of epoxy and Bz can also lead to formation of immobile low molecular weight chains and can possibly induce large areas of chemical heterogeneity in the sample post cure. Although the homopolymerization of Bz is known to give off no volatiles due to its ring opening progression, the curing reaction between Bz and epoxy is significantly more complicated. Lo et. al. found that the type and rate of volatile production in a Bz-epoxy system could be controlled through detailed selection of cure cycle, elevated temperature degassing and Bz-epoxy blend content. It is therefore important to characterize and understand the curing reactions, and in which order they occur in Bz homopolymerization and Bz-epoxy hybrid network formation.

2.4 Curing Process

Curing can be defined as the transition from a liquid state to a 3-dimensional glassy network state [22] . At the initial stage of cure, the blend is composed of monomers, a curing agent, and small chain length oligomers. During cure, two main transition states can be observed: gelation and vitrification. The gel point is defined as the point in time when the polymers, or oligomers, can no longer flow. This state can also be referred to as the rubbery state. After the gel point is reached, mobility of the molecules becomes severely limited [23]. With added thermal energy the system will further crosslink to a glassy state, through a transition known as vitrification. Vitrification occurs when the T_g of the system rises above that of the curing temperature [5]. Time-temperature-transformation (TTT) diagrams are crucial for the understanding of cure in epoxy systems. Within the TTT many states that the curing material will pass through are seen. These include: liquid, sol-glass, sol-gel glass, sol-gel rubber, sol-gel glass, gel-glass and char. Figure 2 displays a common TTT for a thermoset polymer [1]. T_{g0} is defined as the temperature at which no reaction occurs and the system is classified as a sol-glass. T_g^{gel} defines the temperature at which gelation occurs. T_g^{ult} is the maximum T_g that can be reached if the epoxy in the system is fully reacted. When T_g and T_{cure} become the same, vitrification occurs [22]. Crosslinking of thermoset resin networks imparts desirable thermo-mechanical properties and improved chemical resistance [24].

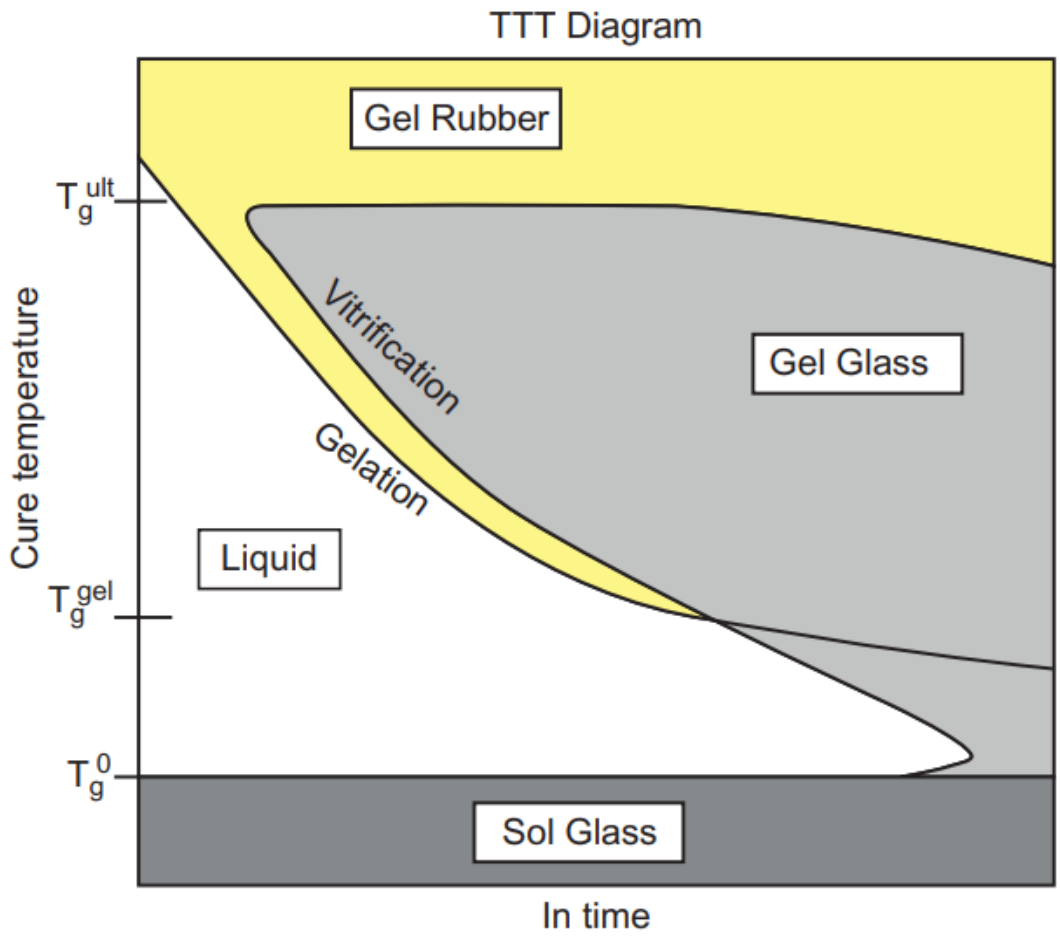

Figure 2: Typical TTT diagram for a thermosetting polymer [1]

2.5 Cure Reaction of Homopolymerized Benzoxazine

The curing reaction of Bz proceeds through ring opening polymerization of the oxazine ring. Residual ring strain acts as a driving force for the ring opening polymerization. Ring opening polymerization is a form of addition polymerization, where monomers join on to the reactive ends of a polymer via ionic propagation. Given the oxazine ring's propensity to open due to residual ring strain, the heat applied during cure will only help to initiate the polymerization. Upon ring opening, a covalent bond is broken and a phenol and amine functionality become available for further reaction and

homopolymerization. Impurities such as phenolic materials from synthesis or other Bz oligomers can act as cationic initiators for ring opening. Pure Bz systems should proceed in a 1:1 manner, with a Mannich bridge forming for every ring that is opened. Dunkers and Ishida proposed a reaction mechanism for protonated Bz which entails the production of an iminium ion as the proton from the nitrogen moves to the oxygen, shown in Figure [3]. This is followed by electrophilic aromatic substitution to the completion of cure [12]. Although nucleophilic ring opening is significantly less common than cationic ring opening, it should be noted that both types of ring opening proceed in parallel during the polymerization of Bz [25].

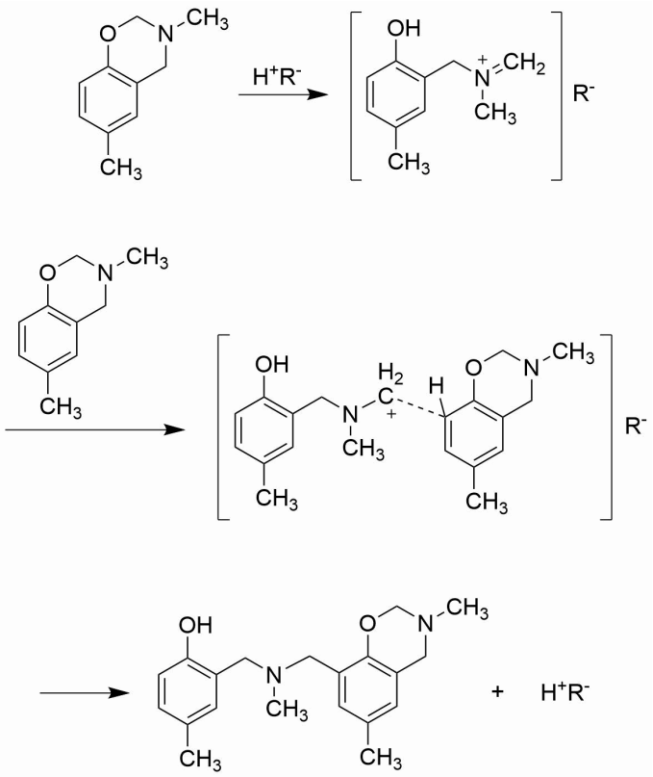

Figure 3: Proposed reaction mechanism by Ishida for Bz homopolymerization. Adapted from [12].

2.6 Cure Reaction of Hybrid Network Benzoxazine-Epoxy Blend

The processing window and variety of thermo-mechanical properties can be controlled through the optimization of epoxy content in epoxy-Bz copolymerized systems. The copolymerization of Bz and epoxy has been explored by many previous researchers [14] [15] [26]. Rimdusit and Ishida investigated the curing of a binary Bz-epoxy system [27]. The differential scanning calorimetry scans showed two significant peaks throughout the cure profile. It is proposed that the first peak originates from reactions between the Bz monomers around 200 ^{o}C, which aligns well with the exotherm observed during cure of a neat Bz monomer. As the oxazine ring is opened, phenolic moieties are formed which catalyze the second reaction of the copolymerization. The proceeding reaction is an etherification reaction, forming an ether link between the epoxide groups and phenyl groups of the Bz. It should also be noted that Rimdusit and Ishida observed an increasing area under the second peak during the non-isothermal differential scanning calorimetry scans, which correlated with an increasing amount of epoxy added to the blend [27].

Ishida and Ohba studied a system of maleimide-functionalized Bz and epoxy. Unlike other binary systems, the maleimide group provides an extra site for crosslinking during polymerization (generally only Bz ring and epoxy ring). The polymerization reactions were observed to occur with use of in-situ FT-IR. They report that epoxy polymerization and Bz polymerization will occur simultaneously, as the generated phenolic groups on the ring opened Bz molecules will act as an initiator and catalyst for the epoxide rings. Ishida and Ohba note that the epoxide bands disappear after only 20 minutes of cure. The maleimide FT-IR peak did not disappear at the end of cure at 240 ^{o}C, which suggests that even higher temperature are required to activate polymerization for

this functionality. The authors also note that the order in which respective functionalities polymerize affects the final properties of the cured blend. In this case the polymerization of the epoxy and Bz occurred first and likely limited the proximity of maleimide groups, hindering their polymerization [28].

2.7 Cure Characterization Methods

There are many techniques which are used to characterize the curing kinetics of thermoset based systems. Some of these techniques include: Fourier Transform Infrared Spectroscopy (FT-IR) [29], Nuclear Magnetic Resonance (NMR) [30], Differential Scanning Calorimetry (DSC) [31], Dynamic Mechanical Analysis (DMA) [32], Thermogravimetric Analysis (TGA) [33], Hybrid Rheometry (HR) [34] and Thermal Mechanical Analysis (TMA) [35]. Of these techniques, this body of work will rely on DSC, DMA, TGA and FT-IR to characterize the cure kinetics and explore the polymerization reactions which occur in a di-functional aliphatic(CER)-BZ blend as well as in a tri-functional glycidyl amine epoxy (TGAP)-BZ system.

2.7.1 Differential Scanning Calorimetry

DSC measures the difference in the heat flow between a pan containing a sample of a known mass, and an empty reference pan. DSC is a widely used thermal characterization technique that allows the user to detect transitions within samples such as T_g, melt temperature, phase changes and curing. The underlying principle is the difference in heat flow to each pan required to keep them at the same temperature. This difference in heat flow, whether it be endothermic or exothermic, will allow for determination of a phase

change or other desired properties [36]. Figures 4 and 5 illustrate a general DSC schematic as well as possible resulting exothermic and endothermic events. In relation to this study, DSC will be used to identify the T_g, heat of reaction, degree of conversion, rate of cure and activation energy. Only non-isothermal scans are conducted in this body of work, however, isothermal scans to determine similar properties related to cure are used commonly.

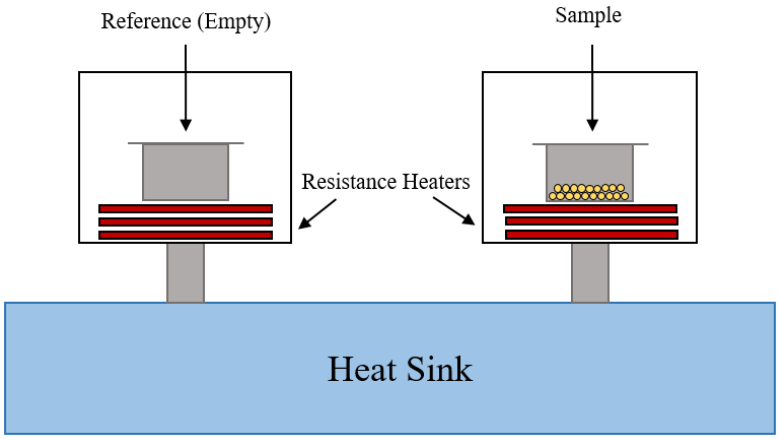

Figure 4: General Schematic for Differential Scanning Calorimetry.

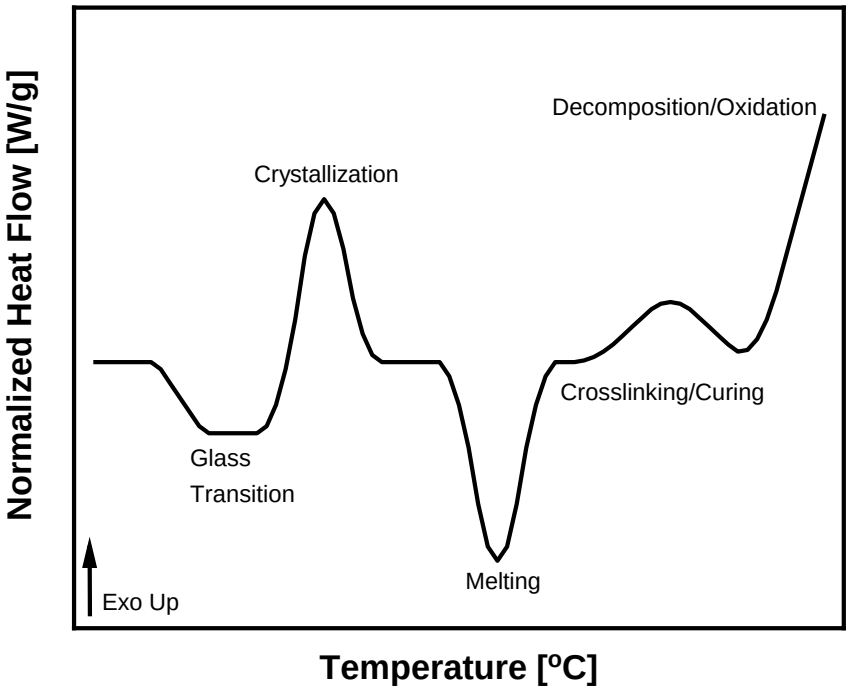

Figure 5: Common exothermic and endothermic events observed from DSC [37].

2.7.2 Dynamic Mechanical Analysis

Dynamic mechanical analysis (DMA) is used to obtain viscoelastic information by applying either a load or a strain to the sample in a sinusoidal manner and monitoring the resulting strain, or load depending on the defined test. DMA measures the stiffness of a material and reports the storage modulus (in phase deformation) and the loss modulus (out of phase deformation) of the material [38]. Tests can be conducted at a static temperature, in a temperature sweep, and oscillatory deformations applied in tension, compression, torsion, or flexural modes. In this work the two properties of interest are the T_g and the crosslink density. T_g can be obtained from the peak of tan delta. Crosslink density can be obtained through use of the storage modulus in the rubbery plateau region located at T_g + 50 ^oC. Equation 1 describes how crosslink density is calculated

$$v = \frac{\rho}{M_c} = \frac{G'}{RT} \quad (1)$$

2.7.3 Fourier Transform Infrared Spectroscopy

In Fourier transform infrared spectroscopy, IR radiation is passed through the sample where some of the radiation will be absorbed. The resulting spectrum collected by the detector is a representative chemical fingerprint of the sample composed of various vibrations and stretches between atoms and bonds.

In-situ FT-IR was employed in this work to track the generation of products and the consumption of reactants throughout the duration of cure. Peak height can be directly related to chemical group concentration through use of the Beer-Lambert Law, shown in Equation 2, where A is absorption, ε is the molar absorptivity coefficient, *l* is the optical path length and *c* is the concentration of the absorbing sample.

$$A = \varepsilon l c \quad (2)$$

A represents absorbance, ε is the molar absorptivity coefficient, *l* is path length and c is the resulting concentration. Absorbance is obtained from peak height, path length can be measured prior to experimentation and molar absorptivity can be calculated from the initial peak height for a specific functional group. Molar absorptivity will be constant throughout the cure cycle, allowing for quantification of the time dependent concentrations and characterization of the cure.

2.8 Cure Kinetic Analysis

Differential scanning calorimetry is the primary technique that will be used for cure kinetic analysis in this work. Isothermal and non-isothermal scans can be performed to obtain kinetic parameters for cure. Isothermal scans involve holding the sample at a given temperature for a set amount of time and monitoring the heat flow. Non-isothermal scans involve heating the sample at a constant heating rate through various temperatures over a given cure cycle. This work will focus on non-isothermal scans to calculate T_g, heat of reaction, max rate of cure, activation energy and degree of cure. The heat of reaction can easily be calculated by integrating the area under the curve of heat flow vs. time for a given cure cycle. Degree of conversion for an epoxy system is defined in Equation 3:

$$\alpha(t) = \frac{H(t)}{H_T} \tag{3}$$

Where α(t) is the degree of conversion as a function of time, H(t) is the current integrated heat flow up to time t and H_T is the total heat of reaction at the completion of cure. Values of α(t) range from 0 at the beginning of a cure cycle, to 1 near the end of the cure cycle.

There are three basic assumptions that need to be made when performing isothermal or non-isothermal kinetic analysis using Differential scanning calorimetry [39]. The first

assumption is that the rate of the kinetic process is proportional to the observed heat flow. Equation 4 shows this relationship where $\frac{d\alpha}{dt}$ represents the rate of the kinetic process, Φ is heat flow and ΔH is the total change in enthalpy throughout the process.

$$\frac{d\alpha}{dt} = \frac{\Phi}{\Delta H} \tag{4}$$

The second assumption is that the rate of the kinetic process can be described by two functions, shown in Equation 5. K(T) is a temperature dependent rate constant and $f(\alpha)$ represents the phenomenological reaction model [39].

$$\frac{d\alpha}{dt} = K(T)f(\alpha) \tag{5}$$

The third assumption to performing isothermal and non-isothermal scans on a DSC is that the temperature dependent rate constant follows and Arrhenius form as shown in Equation 6. A is the pre-exponential factor, E_a represents activation energy, R is the universal gas constant and T is the temperature [39].

$$K(T) = Aexp\left(-\frac{E_a}{RT}\right) \tag{6}$$

Combining Equation 5 and Equation 6 the rate of the kinetic process can be expressed by Equation 7.

$$\frac{d\alpha}{dt} = Aexp\left(-\frac{E_a}{RT}\right)f(\alpha) \tag{7}$$

Substituting $\beta = dT/dt$, Equation 8 for analysis of non-isothermally cured resins can be obtained.

$$\frac{d\alpha}{dT} = \frac{A}{\beta}exp\left(-\frac{E_a}{RT}\right)f(\alpha) \tag{8}$$

2.8.1 Kissinger Method

The Kissinger method allows the kinetic parameters which characterize cure can be obtained from the use of the Kissinger equation with non-isothermal scans. The primary assumption behind this method is that the maximum rate of reaction coincides with the peak temperature of the observed exotherm [40]. The general procedure for the Kissinger method includes performing a set of non-isothermal sweeps at different heating rates and recording the temperature at which maximum heat flow occurs. The Kissinger method is defined in Equation 9. Plotting $\ln\left(\frac{\beta}{T_p^2}\right)$ vs $\frac{1}{T_p}$ allows for the pre-exponential factor, A, and the activation energy E_a to be calculated from the slope and intercept, respectively.

$$\ln\left(\frac{\beta}{T_p^2}\right) = \ln\left(\frac{AR}{E_a}\right) - \frac{E_a}{RT_p} \quad (9)$$

2.9 Objectives

There are a limited number of publications that explore a Bz-CER based system, and even fewer which attempt to explain macro-scale bulk properties using cure behavior and knowledge of the copolymerization. Many research groups within the Bz field of study are focused on tailoring of monomers, and fail to link molecular level observations to bulk scale behavior. The key motivation of this study is to understand the cure behavior of bisphenol-A Bz copolymerized with CER as well as TGAP, and correlate their curing chemistries with bulk scale thermo-mechanical properties.

The main objectives are as follows:

1. Reproduce thermal properties identified in a Bz-CER system explored previously by Barjasteh et. al. [14]
2. Identify an appropriate cure profile for the new Bz-TGAP system with minimal degradation
3. Explain the synergistic increase in T_g observed upon blending Bz-CER and Bz-TGAP
4. Evaluate intramolecular and intermolecular hydrogen bonding via in-situ FTIR scans
5. Explore mechanical properties of cured blends with various wt% epoxy.

In order to achieve these objectives DSC was employed to determine various kinetic parameters, T_g and to help identify an appropriate cure profile for the unexplored Bz-TGAP system. A DMA was also utilized to characterize the viscoelastic properties of the blends as well as the T_g as a function of blend composition and epoxy functionality. FT-IR was

used to track the generation of products and consumption of reactants during cure in order to shed light on a possible reaction mechanism for both Bz-CER and Bz-TGAP systems.

CHAPTER 3

EXPERIMENTAL AND METHODS

3.1 Materials

The three resins used in this study are Bisphenol-A based Bz (tradename Araldite MT35600 CH), CER (tradename Araldite CY 179-1) and a trifunctional triglycidyl epoxy (tradename Araldite MY 0510). All resins were received from Huntsman and used without further purification. After opening, stock monomers were resealed with parafilm and stored in the freezer until further needed. The chemical structures of the Bz and epoxy used are shown in Figures 6, 7 and 8.

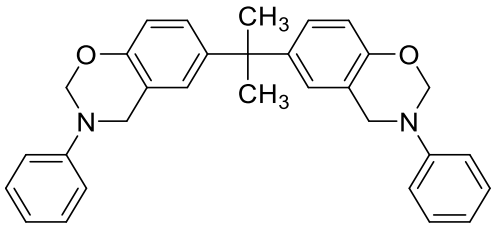

Figure 6: Bisphenol-A Bz.

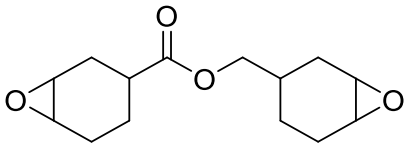

Figure 7: CER Monomer.

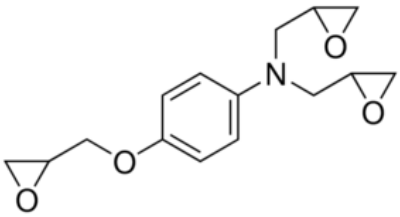

Figure 8: Triglycidyl para-aminophenol (TGAP) Monomer.

3.2 Sample Preparation

The bulk blends were mixed in a rotovap under vacuum at 90°C to ensure the melting and homogenous blending of the Bz with epoxy. Bulk blends were constantly degassed throughout mixing as a vacuum was continuously applied. Blends for both CER and TGAP were mixed at BZ/Epoxy (EP) wt% ratios of 100/0, 75/25, 62.5/37.5, 50/50, 25/75 and the stoichiometric balanced ratio for each epoxy (63.8/36.2 for the CER system, 70.4/29.6 for the TGAP system). The resin mixtures were stored in a refrigerator with parafilm until further needed.

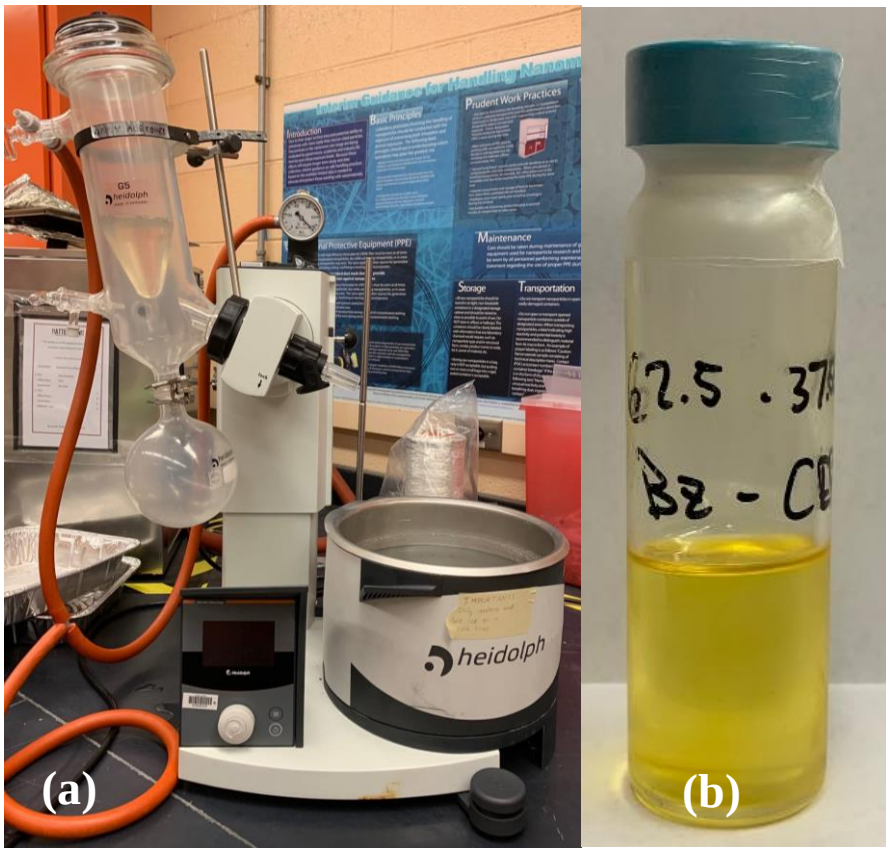

Figure 9: (a) Rotovap used for blending epoxy and Bz at elevated temperature under constant applied vacuum and (b) samples stored in refrigerator with parafilm seal.

3.2.1 Proposed Network Structure

A possible network structure for the homopolymerization of Bz is shown in Figure 10. A possible network structure for the copolymerization of Bz and CER and Bz and TGAP are shown in Figures 11 and 12, respectively. The schematics are representations of small portions of stoichiometric equivalent systems. Red dashed lines represent possible hydrogen bonding sites between two crosslinked monomers. Green dashed lines represent possible hydrogen bonds within the same crosslinked monomer.

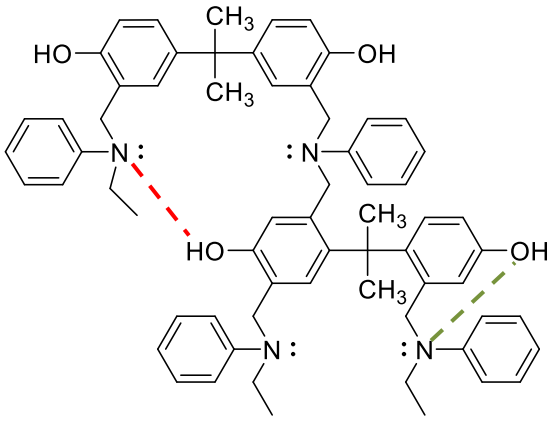

Figure 10: Homopolymerization of 2 Bz monomers.

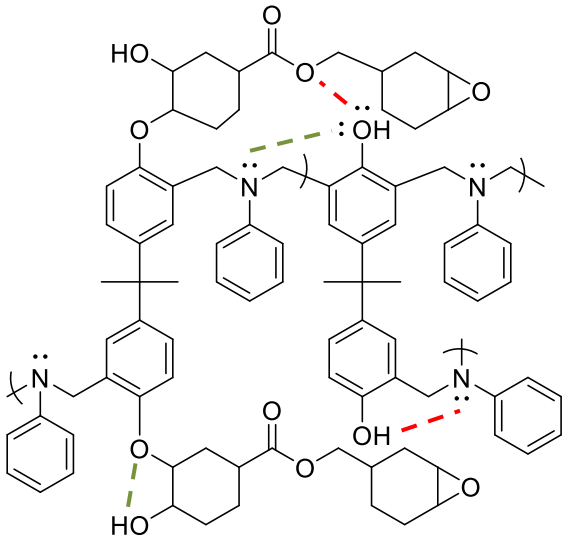

Figure 11: Copolymerization of 2 Bz monomers and 2 CER monomers.

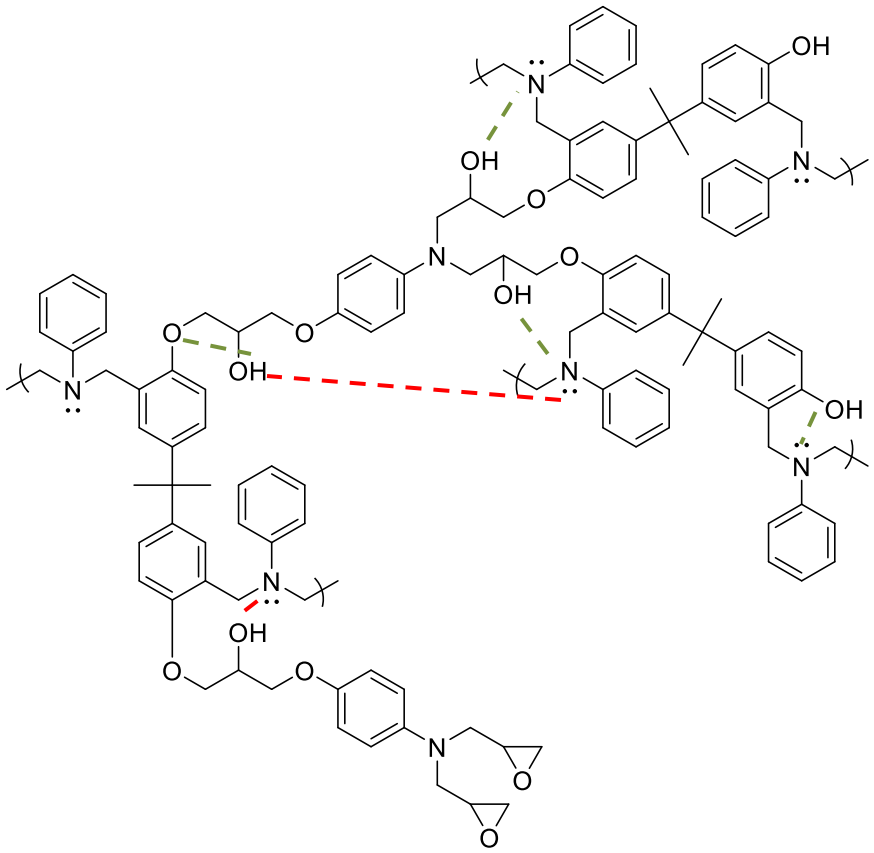

Figure 12: Copolymerization of 3 Bz monomers and 2 TGAP monomers.

3.2.2 Differential Scanning Calorimetry

Three different types of scans were performed using DSC: sweeps for T_g, cure cycles for heat of reaction, and variable heating rate temperature sweeps to calculate activation energy. Aluminum hermetic pans with a pinhole in the lid were used in all cases and the mass of the sample was kept within the range of 5-15 mg. Temperature sweeps for T_g were performed on pre-cured samples. A constant heating and cooling rate of 5 ^oC/min were used to cycle the samples from 30-300 ^oC twice. The first cycle is used to eliminate any thermal history within the sample that may cause undesired exotherms or endotherms in the data. The T_g can be found from the inflection point of heat flow vs. temperature during the second heating cycle of the run, as shown in Figure 5.

For calculating total heat of reaction, uncured resin was used in the sample pan. The samples were cured according to their defined cure cycles in Figure 13. The cure profile for the Bz/CER blends was identified and adapted from the work performed by Barjasteh [14]. Identification of the cure profile for the Bz/TGAP blends will be discussed in Chapter 5. The area under the exothermic peaks was integrated to find the total heat of reaction for each composition.

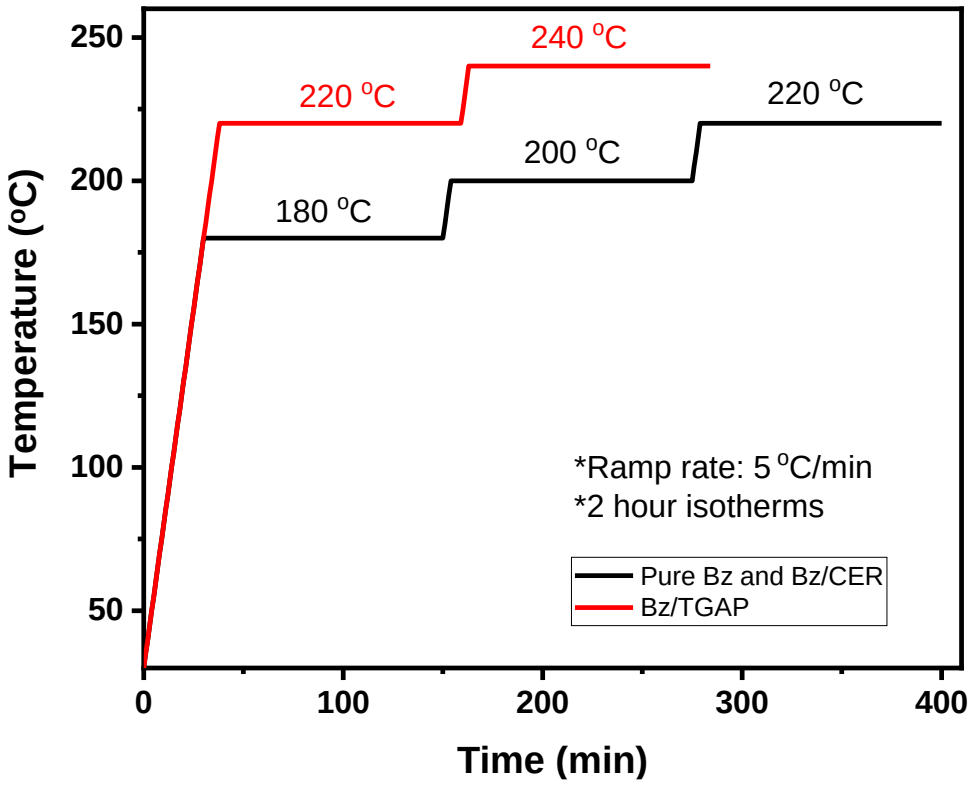

Figure 13: Cure profiles for the various Bz-epoxy systems.

Activation energy was calculated from five separate temperature sweeps from 30 °C -300 °C at heating rates of 1 °C/min, 2 °C/min, 5 °C/min, 10 °C/min and 20 °C/min. The peak temperatures for each exotherm are used in the Kissinger method [40] to calculate activation energy.

Figure 14: (a) Discovery DSC 2500 and (b) Hermetic aluminum pinhole DSC pan and lid.

3.2.3 Thermogravimetric Analysis

Thermogravimetric Analysis (TGA) was used to characterize the thermal stability of certain Bz/TGAP blends. 5-10 mg of sample was placed in a platinum pan, and a temperature sweep from 30-900 ^{o}C was performed at 5 ^{o}C/min in an air environment. Degradation onset temperatures were recorded at 5 wt% sample mass loss.

Figure 15: TGA Q500 used for thermal stability measurements.

3.2.4 Dynamic Mechanical Analysis

Pre-mixed resin blends were removed from the refrigerator and heated to 100-120 ^{o}C, depending on their Bz content, in preparation for pouring. Samples with higher wt% Bz were significantly more viscous at lower temperatures. Molds were kept in a vacuum oven at 130 ^{o}C to preheat and facilitate minimization of bubbles during pouring. Once the blends were workable, they were poured into two different molds, one for tension and one for torsion. One interesting note is that all the Bz-TGAP blends cured with a rippled surface, while the neat Bz and Bz-CER systems cured with a smooth glass-like surface as shown in Figure 17.The dimension of the tension mold is 60 mm x 6.5 mm x 1.5 mm. The dimension of the torsion mold is 70 mm x 14 mm x 3 mm. Samples were degassed at 130 ^{o}C for 20-30 minutes until there were no visible bubbles and placed in a programmable oven for cure. Cure profiles for each system follow those defined in Figure 13. Post cure, the samples were face-milled to eliminate any distortions on the surface of the sample. Samples were polished with 600 grit sandpaper prior to testing. During DMA testing, the tensile based specimen generated significant amounts of noise after its T_g was passed. This issue was solved by switching to only torsional mode testing for the rest of characterization. Torsional DMA measurements were performed within the linear viscoelastic region with a strain amplitude of 0.05%, a frequency of 1 Hz with a temperature ramp from 30-300 ^{o}C at 5 ^{o}C/min. To define the linear viscoelastic region strain amplitude, sweeps were conducted at room temperature, a frequency of 1 Hz and between 0.001% and 1% strain amplitude.

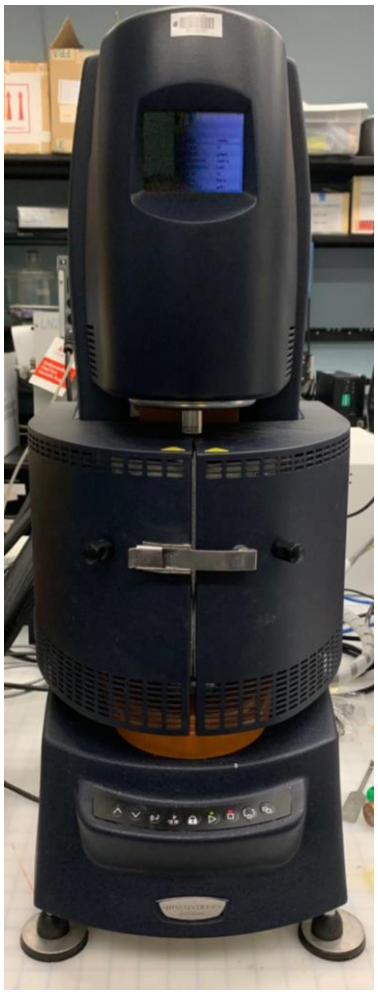

Figure 16: Discovery Series Hybrid Rheometer used for DMA measurements.

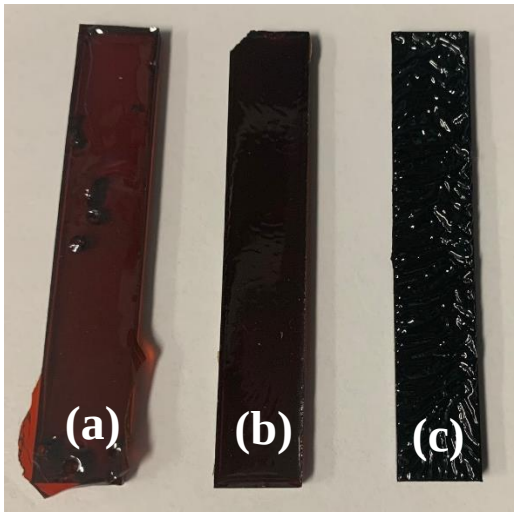

Figure 17: Torsional DMA bars. (a) Pure Bz, (b) 75/25 (Bz/CER), (c) 75/25 (Bz/TGAP).

3.2.5 Tensile Testing

Five dogbones were prepared for each blend in accordance to ASTM D638-V. The geometry of the dogbone molds are as follows: depth of 3.4 mm, gage width of 3 mm, tab width of 9.5 mm and length of 64 mm. Post cure samples were face-milled to eliminate any surface deformities and polished with 600 grit sandpaper parallel to the direction of test.

Figure 18: Post-test dogbone.

3.2.6 Fourier-Transform Infrared Spectroscopy

Mid *in-situ* FT-IR were performed for all blends of neat, CER and TGAP systems. Salt discs 2mm in thickness were used to enclose a small amount of material for MIR scans with a path length of 0.003 cm. Mid-IR scans were performed over the range 700-4000 cm^{-1}, averaging 32 scans every 2 minutes for the duration of the cure cycle. Figure 19 shows the FT-IR and heated cell that were used for in-situ data collection. Figure 20 shows preparation of MIR samples. The collection of CSV files after each run was combined in Origin into a set of hyper-spectral data and further analyzed in Matlab using peak height tracking scripts.

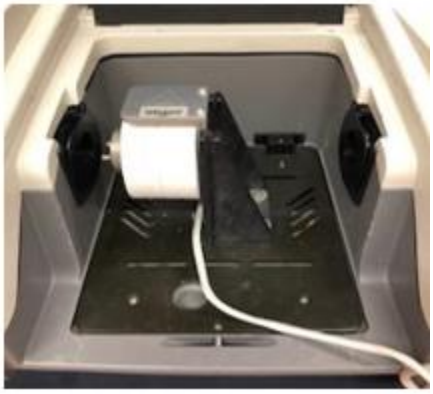

Figure 19: FT-IR chamber with fitted in-situ heating cell.

Figure 20: MIR sample prep between two 2mm salt discs.

CHAPTER 4

NON-ISOTHERMAL CURE KINETICS AND MECHANICAL DATA OF BENZOXAZINE/DI-FUNCTIONAL CYCLOALIPHATIC EPOXY

4.1 DSC Characterization

4.1.1 Glass Transition Temperature

The motivation for investigating this specific Bz-CER system comes from the work performed by Barjasteh et. al. [14]. Their work focuses on characterizing the activation energies and heats of reaction of Bz-CER systems via isothermal and nonisothermal temperature ramps, as well as brief characterization via DMA. In this study, Bz-CER samples were made at five different weight percentage ratios of (Bz/CER) 100/0 (neat), 75/25, 63.8/36.2 (stoichiometric), 62.5/37.5, 50/50 and 25/75 (epoxy rich blend). These compositions were chosen to mirror those studied in the experiments performed by Barjestah. Two additional compositions were considered: the stoichiometric equivalent and a very epoxy rich composition of 25/75, to compliment the work performed in Barjasteh's study. Figure 21 illustrates the DSC temperature sweeps used to identify the T_g of each blend. Samples were thermally cycled twice, the first cycle used to alleviate thermal history from processing.

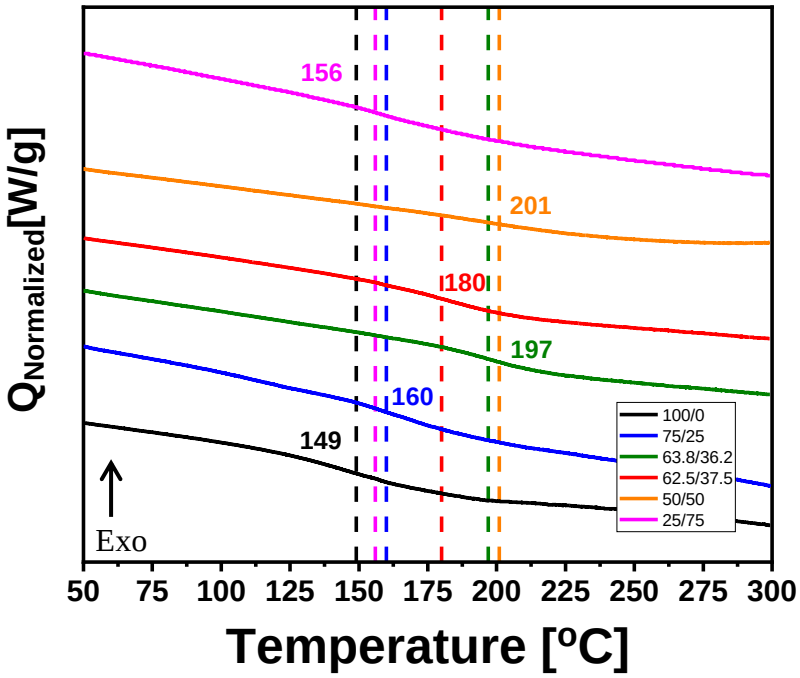

Figure 21: T_g sweeps for neat Bz and Bz/CER Blends.

Table 2: T_g as a function of CER wt. %.

Composition (Bz/Ep) [wt%]	T_g [ºC]
100/0	149
75/25	160
63.8/36.2	197
62.5/37.5	180
50/50	201
25/75	156

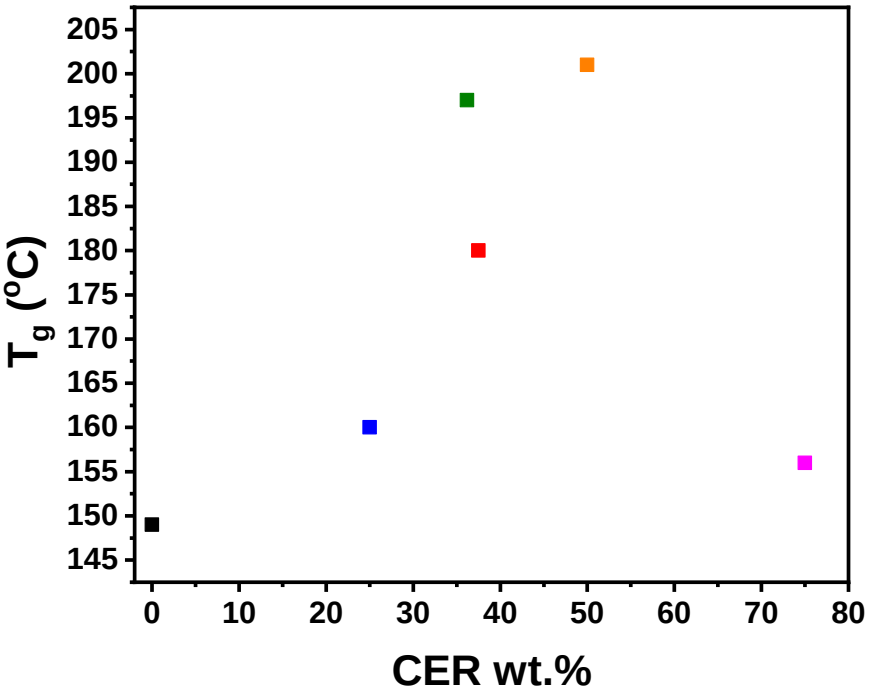

Figure 22: Tg vs CER wt. %.

Figure 22 and Table 2 show the T_g's obtained from differential scanning calorimetry of various weight percentage blends**.** The blends appear to have lower glass transitions when dominated by only epoxy or only Bz. The highest performing blend exhibited a T_g of 201 °C at a 50/50 ratio, closely followed by the stoichiometric equivalent (63.8/36.2) with a T_g of 197 °C. When an excess amount of epoxy by weight was introduced, well beyond the stoichiometric equivalent, blends likely did not fully cure due to an imbalance between reactive sites on the epoxy and Bz, explaining their low T_g's. It should be mentioned that when CER is cured with a common curing agent such as hexahydrophthalic anhydride T_g values of 150-160 °C can be obtained [41].

4.1.2 Heat of Reaction

Heat of reaction was calculated for each blend by subjecting an uncured resin sample to the predefined cure cycle on the DSC. The total heat of reaction is calculated by

integrating the area under the curves during the three isothermal holds. The same cure profile was used in this study as in the study performed by Gouni and Barjasteh [26].

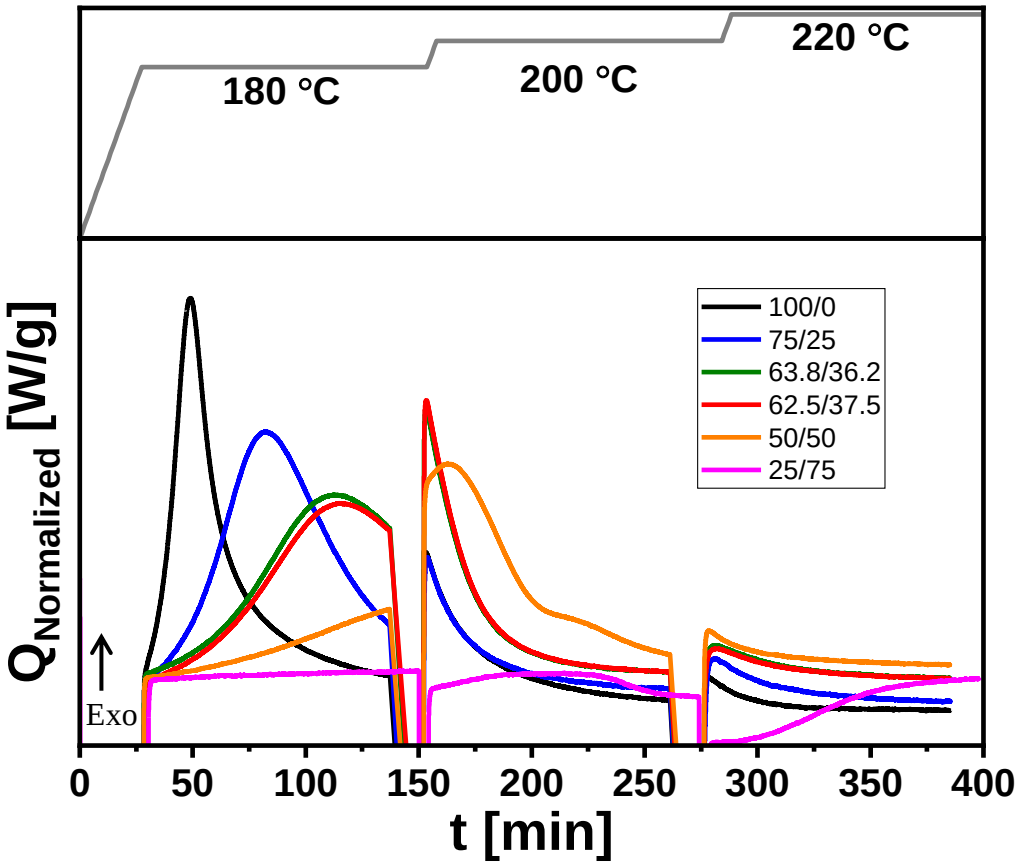

Figure 23: DSC Temperature sweep over defined Bz/CER cure profile.

Table 3: Heat of Reaction for Neat Bz and Bz/CER Blends.

Composition (Bz/EP) (wt%)	ΔH (J/g)	ΔH (J/g) Barjasteh [14]
100/0	337	342
75/25	405	399
63.8/26.2	359	N/A
62.5/37.5	335	N/A
50/50	260	296
25/75	75	N/A

Figure 23 displays the cure profile and resulting normalized heatflow obtained from the DSC for each composition. Heat of reactions were also measured by Gouni and Barjasteh and are shown for comparison in Table 3. The values obtained in this study appear to match closely with those obtained by Gouni and Barjasteh. In this study, upon addition of 25 wt.% CER, the heat of reaction increased by ~20%.

4.1.3 Degree of Conversion

Degree of conversion is calculated by integrating the current heat flow from time 0 to time t and dividing by the total heat of enthalpy measured for the reaction. Total heat of enthalpy is defined as the area under the DSC thermograms at the completion of the defined cure cycle. Equation 3 is used to calculate degree of conversion for various Bz/Ep blends. Degree of conversion should not be confused with degree of cure. Figure 24 shows all conversions finishing at 100%, because they are normalized to their own maximums. The purpose of Figure 24 is to show relative rates of cure throughout the three two-hour isotherms. As the wt% epoxy increases, the degree of conversion trends downward during the first isotherm, and some of the exothermic curing activity begins shifts to the second isotherm at 200 ^{o}C. This is consistent with the trend observed in Figure 23.

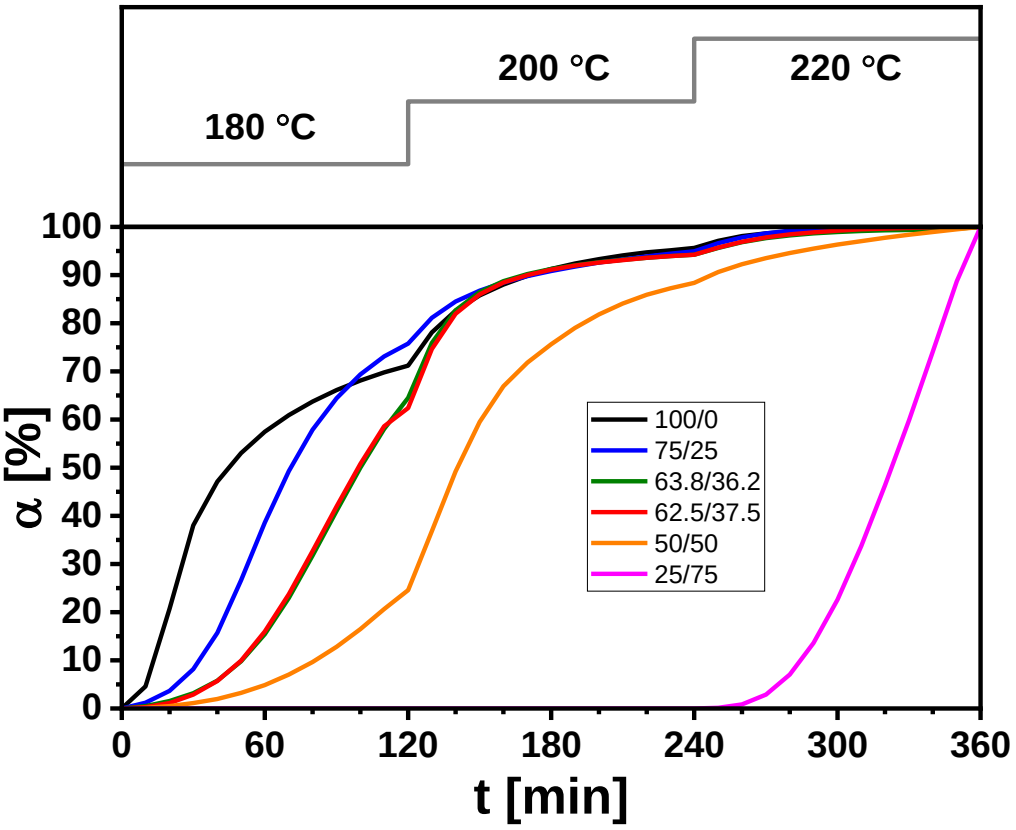

Figure 24: Degree of Conversion for Neat Bz and Bz/CER Blends.

4.1.4 Activation Energy: Kissinger Method

The Kissinger method is defined in Equation 9. The general procedure includes performing a set of non-isothermal sweeps at different heating rates and recording the peak temperature at which maximum heat flow occurs. Plotting $\ln\left(\frac{\beta}{T_P^2}\right)$ vs. $\frac{1000}{T_P}$ allows activation energy to be obtained from the slope, and the pre-exponential factor from the intercept. Figure 25 shows the Kissinger relation for each wt% blend at 1, 2, 5, 10 and 20 °C/min and the resulting activation energies are calculated in Table 4. Gouni and Barjasteh performed activation energy measurements on some of the Bz-CER blend compositions that this study

focuses on. The results from their work are shown in Table 4 for comparison. There does not appear to be a significant increase in activation energy upon addition of CER.

Table 4: Calculated Activation Energy for neat Bz and Bz/CER Blends.

Composition (Bz/Ep) [wt.%]	Activation Energy [kJ/mol]	Activation Energy [kJ/mol] [26]
100/0	86.1	92.3
75/25	94.4	96.5
63.8/36.2	96.3	N/A
62.5/37.5	95.2	N/A
50/50	106.9	96.35

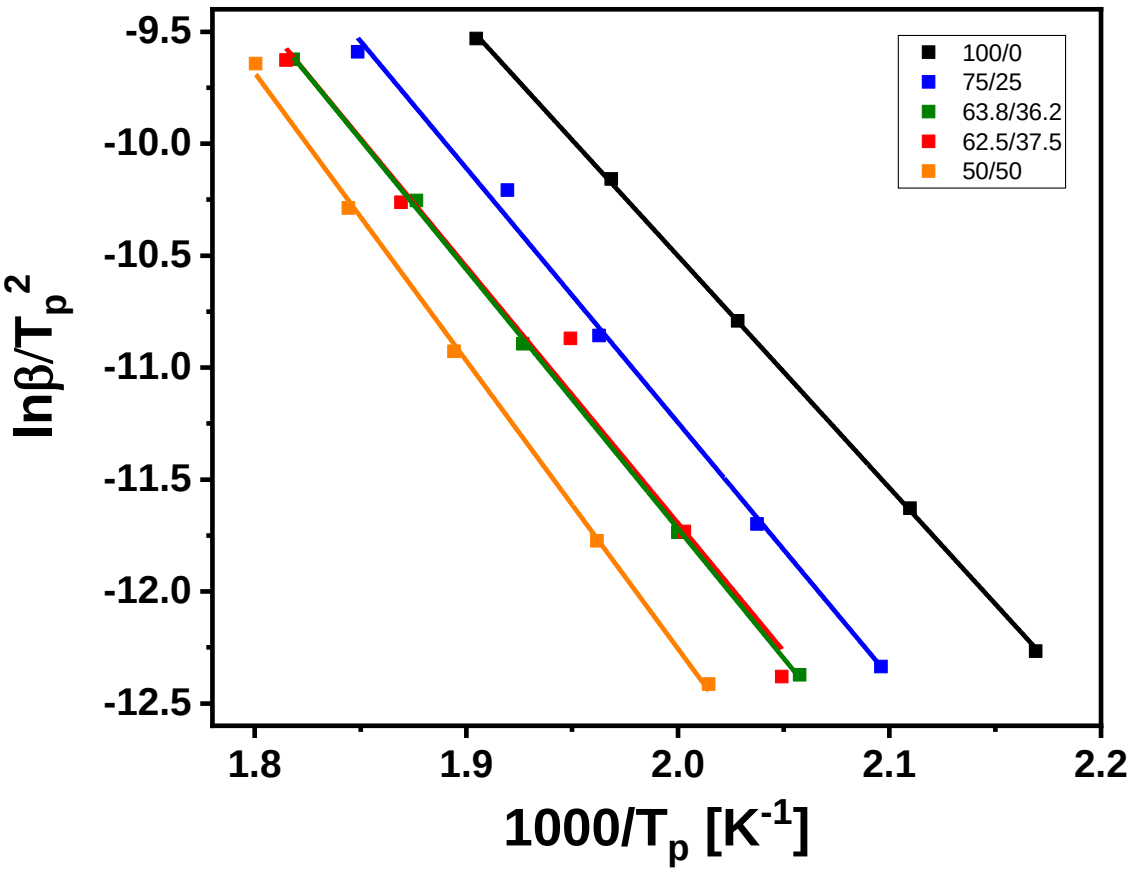

Figure 25: Kissinger method plots for Activation Energy of Neat Bz and Bz/CER Blends.

4.2 DMA Characterization

Samples were tested for T_g's, and crosslink densities were calculated from the rubbery plateau modulus located at T_g + 50 ºC. The glass transition of a polymer is the temperature region in which the polymer changes from a glassy state to a rubbery state. T_g can be defined as the peak of the tan(δ) curve, at which there is a significant increase in the segmental motion of the polymer backbone. Tan(δ) is defined in Equation 10. Tan(δ) for each blend is shown in Figure 26 and accompanying T_g's in Table 5 and Figure 27.

$$tan(\delta) = \frac{G''}{G'} \tag{10}$$

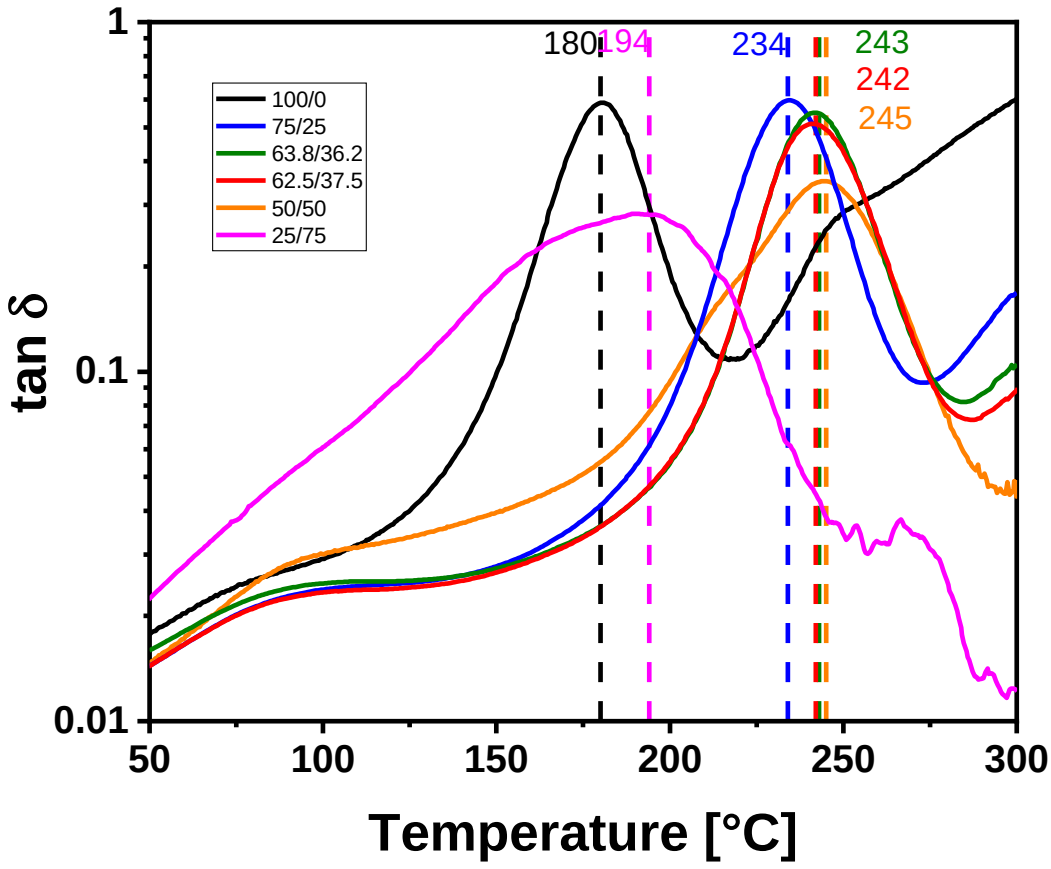

Figure 26: Temperature sweeps for glass transition of neat Bz and Bz/CER blends.

Table 5: T_g via DMA.

Composition (Bz/Ep) [wt%]	T_g [ºC]	T_g [ºC] [14]
100/0	180	169
75/25	234	233
63.8/36.2	243	N/A
62.5/37.5	242	257
50/50	245	226
25/75	194	N/A

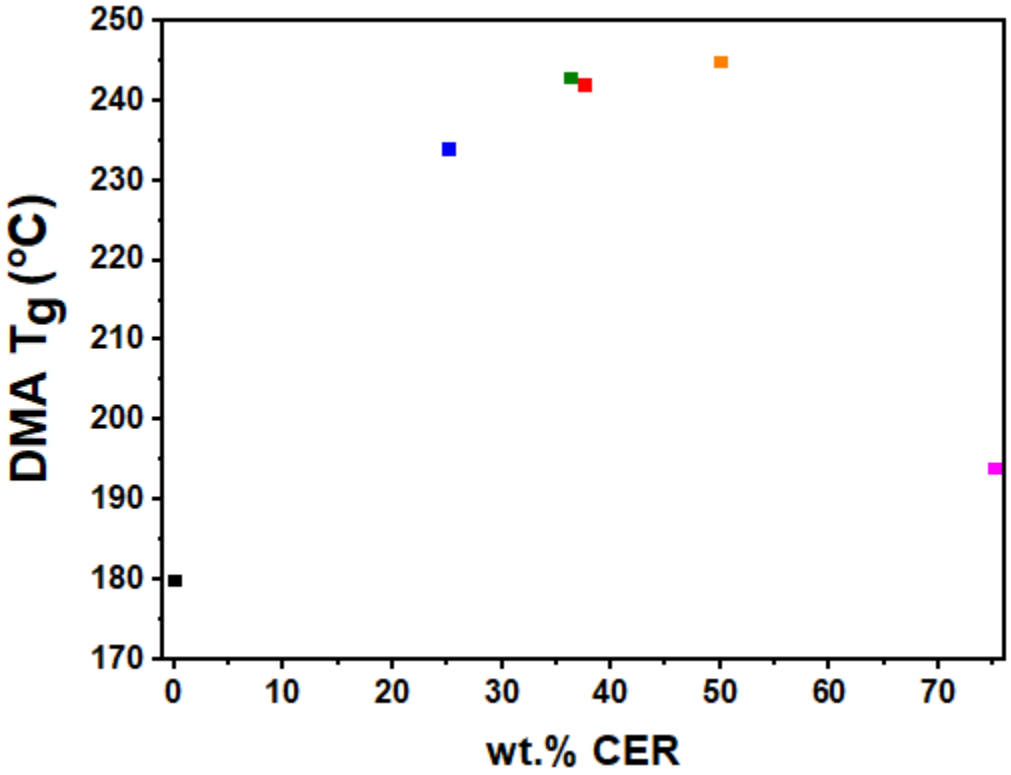

Figure 27: T_g vs. wt. % CER via DMA.

The T_g's of the blends increase with increasing epoxy content, up to 75 wt.% CER. The lowest T_g is exhibited by neat Bz, and a maximum T_g is achieved at a ratio of 50/50 Bz/Ep. A gap of ~70 ºC exists between the neat Bz and the blend with the highest glass transition. The T_g's obtained via DMA are on average 30-40 degrees higher than those measured via DSC, however a similar trend of increasing T_g upon addition of even 25 wt.%

CER is observed. Additionally, the T_g's via DMA of the blends centered around the stoichiometric equivalent are very close to each other, like the trend observed via DSC measurements. It is likely that the 25/75 blend did not contain a high enough wt. % of Bz to fully react with the epoxy, leaving the system in a severely under cured state. Another notable observation that can be derived from the plots of tan(δ) is the broadening of the peak at 75 wt.% CER. A broad tan(δ) peak signifies a wide range of relaxations within the sample. This could likely be attributed to a heterogeneous crosslinked network, with crosslink density being higher in some locations of the sample and lower in others.

Storage and loss modulus curves via torsion are shown in Figure 28; values at 35 ^{o}C are shown in Table 6. Equation 1 describes how crosslink density is calculated.

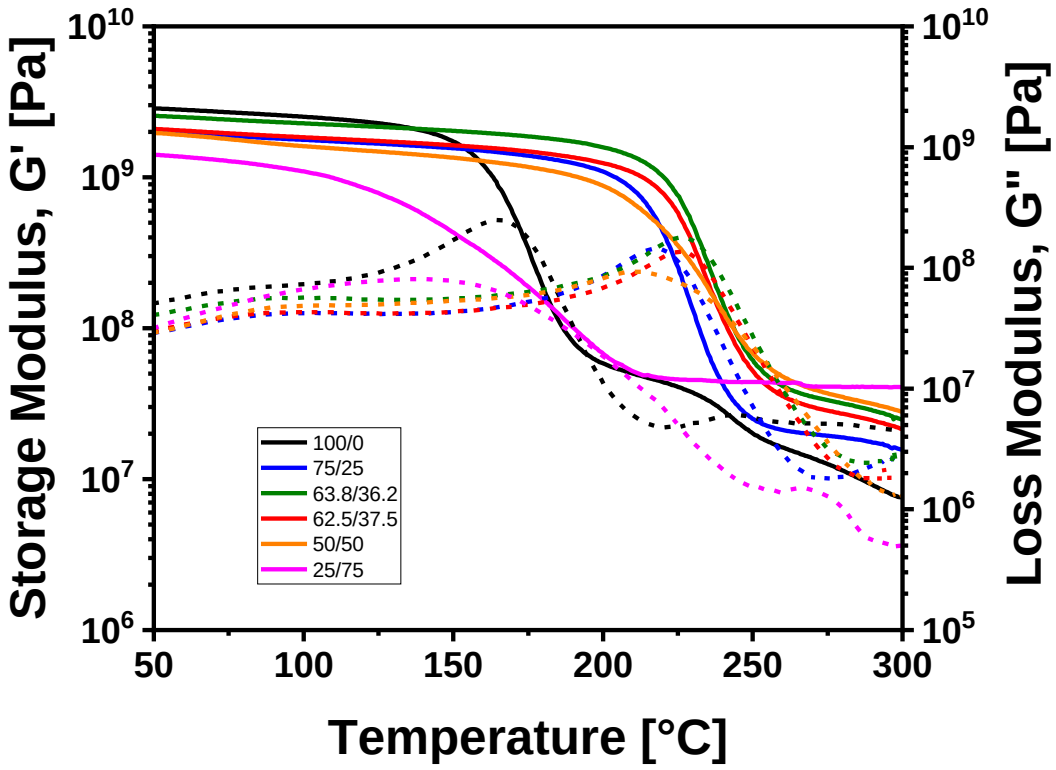

Figure 28: Temperature sweeps for Storage Modulus and Loss Modulus of Neat Bz and Bz/CER Blend.

Table 6: Storage Modulus, Loss Modulus and Crosslink Density of Neat Bz and Bz/CER Blends.

Composition (Bz/Ep wt%)	G'(35 ºC) [GPa]	G"(35 ºC) [MPa]	ν [mol/m^3]	ν [mol/m^3] [14]
100/0	3.0	42.8	2750	1925
75/25	2.1	25.8	3967	2953
63.8/36.2	2.6	38.5	5848	N/A
62.5/37.5	2.2	26.2	5069	3445
50/50	2.0	25.7	6330	5178
25/75	1.5	24.2	10237	N/A

Modulus appears to decrease upon the initial addition of CER into the system. The stoichiometric blend exhibits a modulus near that of the neat Bz, likely due to a balance of the reactive sites, and a reduction in the amount of not fully cured short chain length oligomers. The modulus of the 25/75 blend is significantly lower than that of the neat Bz or any of the other blends, this is in line with the results from calculating heats of enthalpy and can possibly be explained by the hindering of the cure reaction and reduction in the overall homogeneity of the crosslink network. Given the blend is so far from its stoichiometric equivalent, the final cured product may exhibit pockets or nodules of heterogeneity that detrimentally affect mechanical properties. This claim is further evidenced by the broadening of the tan(δ) curve of the 25/75 Bz/CER system. Crosslink density follows a similar trend as modulus, excluding the 25/75 blend crosslink density. It is possible that the 25/75 system undergoes additional curing during the DMA testing, causing the DMA results to be inaccurate for this single blend. Barjasteh et. al. also calculated crosslink densities for some of the compositions explored. The trend observed in this study matches the increasing crosslink density upon addition of CER that Barjasteh et. al. recorded. It should be noted that the neat benzoxazine does not exhibit a rubbery

plateau region at T_g + 50 °C, therefore the crosslink density calculation for the 100/0 sample should also be calculated using other methods to ensure its validity.

4.3 Tensile Characterization

Table 7: Average Stress, Strain and Modulus for neat Bz and Bz/CER Blends.

wt. % CER	Modulus [GPa]	UTS [MPa]	Strain at Failure [%]
100/0	4.1 ± 0.1	52.3 ± 11	1.4 ± 0.5
75/25	5.0 ± 0.1	49.2 ± 10	1.1 ± 0.3
63.8/36.2	4.3 ± 0.2	33.9 ± 7.3	0.8 ± 0.2
62.5/37.5	5.0 ± 0.2	48.7 ± 3.7	1.1 ± 0.1
50/50	4.7 ± 0.2	34.5 ± 13	0.8 ± 0.3
25/75	4.9 ± 0.4	30.1 ± 3.2	0.7 ± 0.0

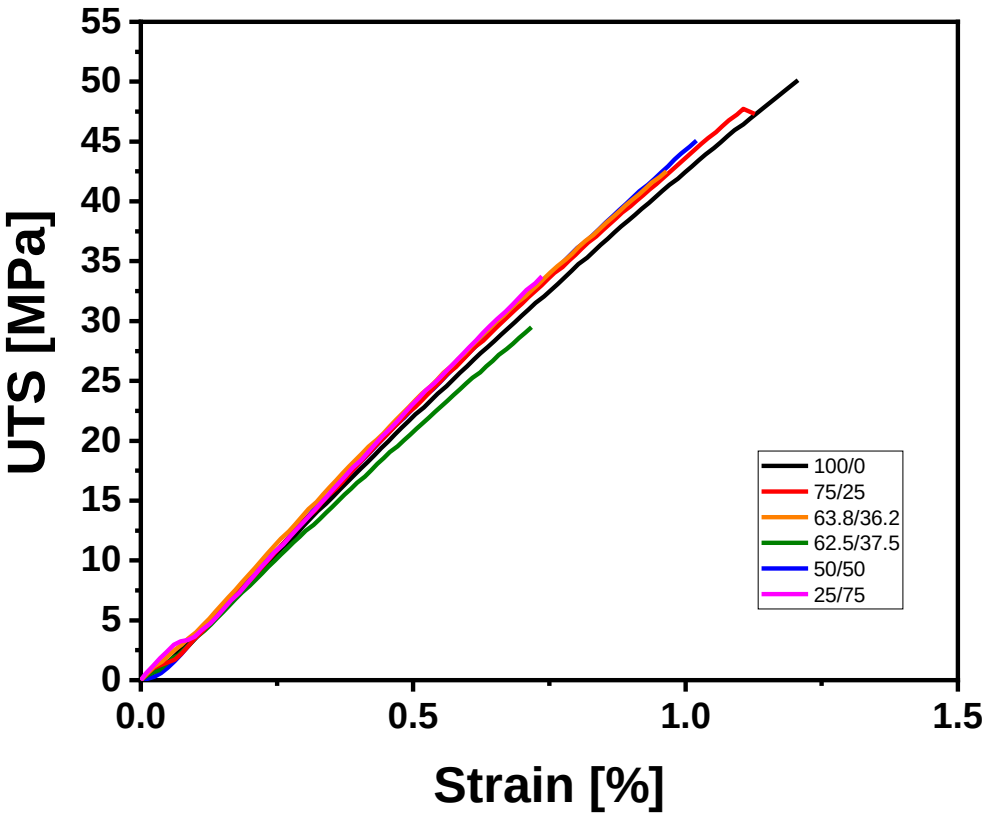

Figure 29: Representative Stress-strain curves for neat Bz and Bz/CER Blends.

Tensile strength of neat benzoxazine was found to be 52.3 ± 11 MPa and decreased to 30.1 ± 3.2 MPa with the addition of epoxy up to 75 wt.% CER. Barjasteh reported a maximum tensile strength for neat Bz of 69 MPa and a minimum tensile strength of 39 MPa at 50 wt.% CER.

Strain to failure for neat Bz was 1.4 ± 0.5 %. It is difficult to comment on the trend of strain to failure as all values are similar, and many are within error of each other. Barjasteh et. al. reported an increasing strain to failure with added epoxy. The minimum strain to failure of 1.9% was reported for neat Bz, with strain to failure increasing to 2.7% upon addition of 50 wt.% CER.

Tensile modulus of neat Bz was measured to be 4.13 ± 0.09 GPa and increased 20% to 4.97 ± 0.09 when 25 wt.% CER was introduced. There does not appear to be a significant trend in the tensile modulus past 25 wt.% CER, with moduli for samples containing greater than 25 wt.% CER exhibiting variable moduli from 4.34 - 4.97 GPa. Barjasteh et. al reported a decrease in modulus from neat Bz at 4.1 GPa to 2.7 GPa at 50 wt.% CER. The increase in modulus in this study could be explained by the increased crosslink density when CER is introduced into the Bz system.

4.4 FT-IR Characterization

Mid-range (4000-700 cm^{-1}) *in-situ* FT-IR hyperspectral analysis was performed for all Bz/CER blend ratios. Salt discs 2mm in thickness were used to enclose a small amount of material with a path length of 0.003 cm for MIR scans. Mid-IR scans were performed over the range 700-4000 cm^{-1} w, averaging 32 scans every 2 minutes for the duration of

the cure cycle. FT-IR was also conducted on uncured monomers to identify characteristic peaks.

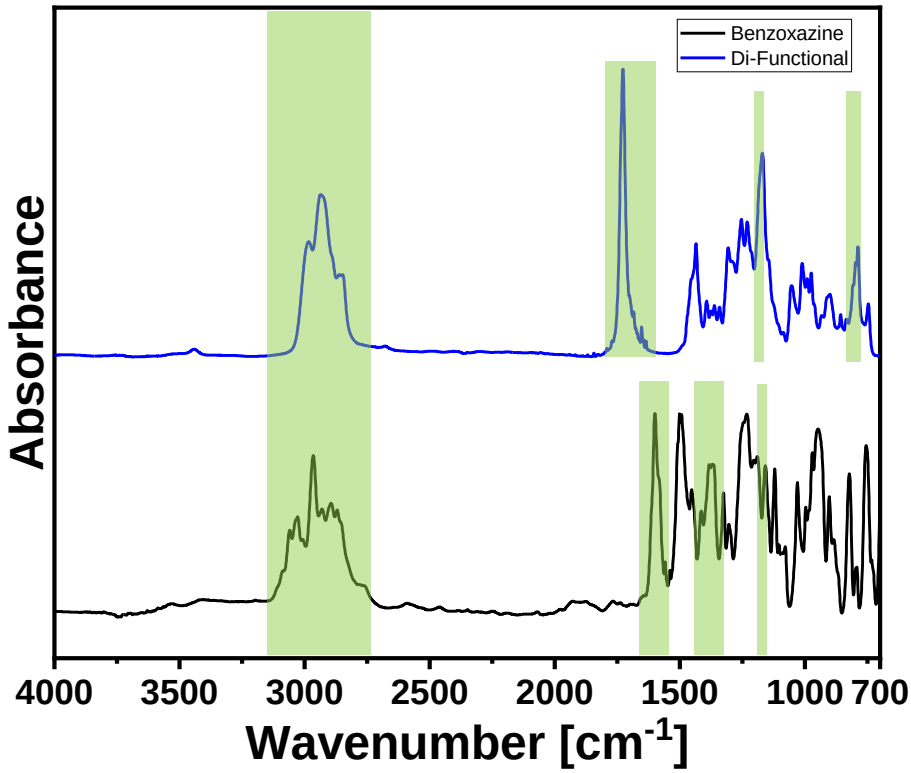

Figure 30: Mid-IR of uncured neat monomers from 700 cm-1 to 4000 cm-1.

Single FT-IR scans taken on uncured monomer are shown in Figure 30. In the neat Bz monomer there are several peaks of interest. CH stretching can be seen across the wavenumber range of 2665-3150 cm^{-1}. Stretching of the oxazine ring is observed at 945 cm^{-1}. N-C-O stretch is visible at 1600 cm^{-1}, C-O-C stretch at 1160 and CH_2 wagging into a closed oxazine ring at 1362 [42]. No hydrogen bonding peaks are observed in the range 3300-3600 cm^{-1} [29] [43].

The uncured CER exhibits 4 strong characteristic peaks. Stretching of the epoxide group can be seen at 790 cm^{-1}, CH stretch within the range of 2665-3150 cm^{-1}, C-O-C stretch at 1170 cm^{-1}, and a C=O stretch at 1730. These peaks are observed throughout the

cure, however, their relative intensities are found to decrease by the end of the implemented cure cycle.

First and last spectra from in-situ FTIR are shown in Figure 31. The homopolymerization of Bz during cure is known to proceed in a ring opening manner. The proposed mechanism includes opening of the oxazine ring at the N-C-O bond as illustrated in Figure 32. The oxazine ring stretch can be seen at 945 cm^{-1} and the N-C-O stretch is located at 1600 cm^{-1}. The N-C-O ring opening polymerization is confirmed by the decrease in absorbance post-cure of both peaks mentioned prior.

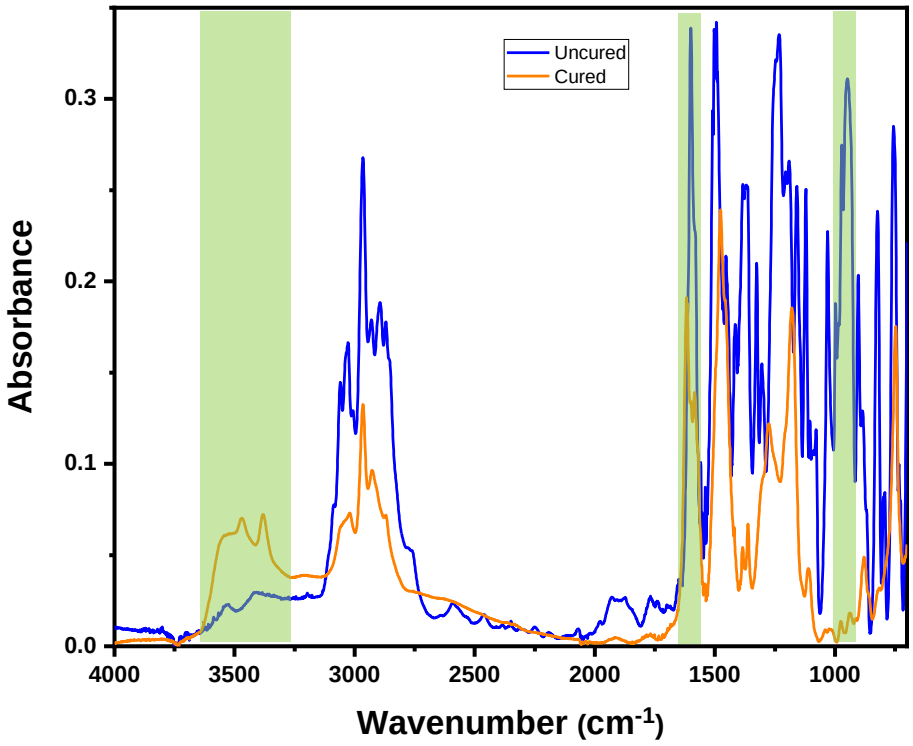

Figure 31: FT-IR Spectra of homopolymerized Bz.

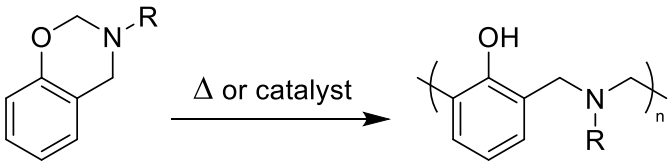

Figure 32: Bz homopolymerization mechanism.

As a result of the oxazine ring opening, intra- and inter-molecular hydrogen bonds will start to form. As evidenced in Figure 31, distinct peaks in absorbance after cure can be seen at 3370 cm^{-1}, 3470 cm^{-1} and 3560 cm^{-1}. The peak at 3370 cm^{-1} corresponds to intermolecular hydrogen bonding between dangling OH groups and oxygen atoms on unopened oxazine rings. Intramolecular hydrogen bonding between the same dangling OH groups and oxygen atoms of the unopened oxazine ring is also seen at 3470 cm^{-1}. OH-π intramolecular hydrogen bonding is also observed at the 3560 cm^{-1} [29].

First and last spectra from in situ FT-IR of the stoichiometrically balanced Bz/CER blend is shown in Figure 33. The hybrid network is formed initially through the ring opening polymerization of the Bz. As OH sites become available via the opening of the oxazine ring, the epoxide groups from the CER can readily crosslink into the network. The proposed mechanism is shown in Figure 34.

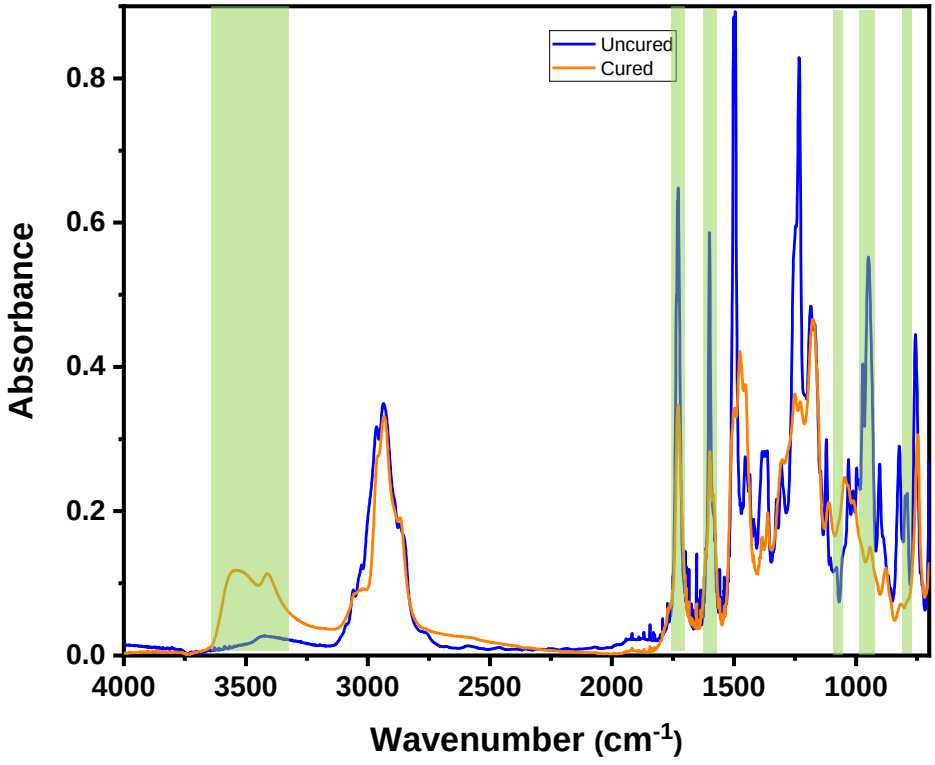

Figure 33: FT-IR Spectra of Bz/CER stoichiometric blend.

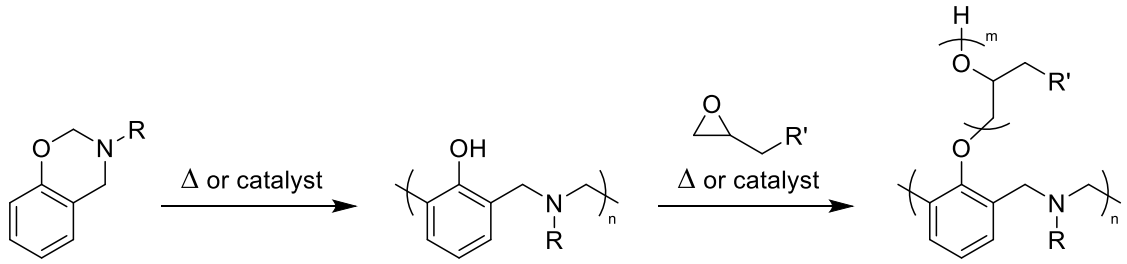

Figure 34: Bz/Epoxy hybrid network formation.

The FT-IR of the blend in Figure 34 exhibits peaks at similar wavenumbers as the homopolymerized Bz. The consumption of the oxazine ring is seen at 943 cm^{-1} and is also shifted two wavenumbers from the homopolymerized system. The N-C-O stretch located at 1600 cm^{-1} is also visible and decreases in absorbance as cure proceeds, signifying crosslink formation with other Bz monomers or CER monomers. Peaks that are unique to the CER include: C-O-C stretch at 1120 cm^{-1}, epoxide stretch at 790 cm^{-1} and bound C=O stretch at 1728 cm^{-1}. All three of these peaks are observed to decrease in absorbance post cure, signifying that the CER was consumed in hybrid network formation. Product peaks include Intermolecular OH-O hydrogen bonding at wavenumber 3400 cm^{-1} and intramolecular OH-π hydrogen bonding at 3540 cm^{-1} [29]. The lack of a peak at 3470 cm^{-1}, signifying intramolecular OH-O hydrogen bonding, can likely be explained by the increased availability of intermolecular hydrogen bonding sites present by the added CER.

4.5 Summary and Conclusions

All of the Bz/CER blends exhibited an increase in T_g via DSC and DMA upon addition of CER. The 50/50 blend exhibited the highest T_g of 245 ^oC, followed closely by the 62.5/37.5 blend at 242 ^oC and the stoichiometric equivalent (63.8/36.2) blend at 243

^{o}C. Crosslink density was found to increase from 2750 mol/m^3 in neat Bz to 10237 mol/m^3 as up to 75 wt.% CER was added.

One noticeable downside to the 25/75 and 50/50 blend is that the tan(δ) peak is broad, signifying a heterogenous network with variable crosslink density. This type of curing behavior is undesirable and removes the 25/75 and 50/50 composition from the list of optimal blends. The activation energies for all compositions are roughly the same for the Bz/CER system.

It is difficult to pick out a blend which performed significantly better than the other in regards to tensile properties, as many of the measured values are within error of each other. Taking this into consideration, the stoichiometric equivalent blend should be selected as the most optimal blend given its relatively high T_g and higher propensity for completion of cure with balanced reactive groups (oxazine and epoxide).

CHAPTER 5

NON-ISOTHERMAL CURE KINETICS AND MECHANICAL DATA OF BZ/TRI-FUNCITONAL TRIGLYCIDYL EPOXY

5.1 Cure Profile Identification

In order to properly characterize the Bz/TGAP system, a suitable cure profile needed to be defined. To begin with, the cure profile identified by Barjasteh et. al. [14] for Bz homopolymerization and Bz/CER copolymerization was implemented. This cure profile was used for all Bz/CER compositions in Chapter 4. The resulting DSC exotherms are shown in Figure 35.

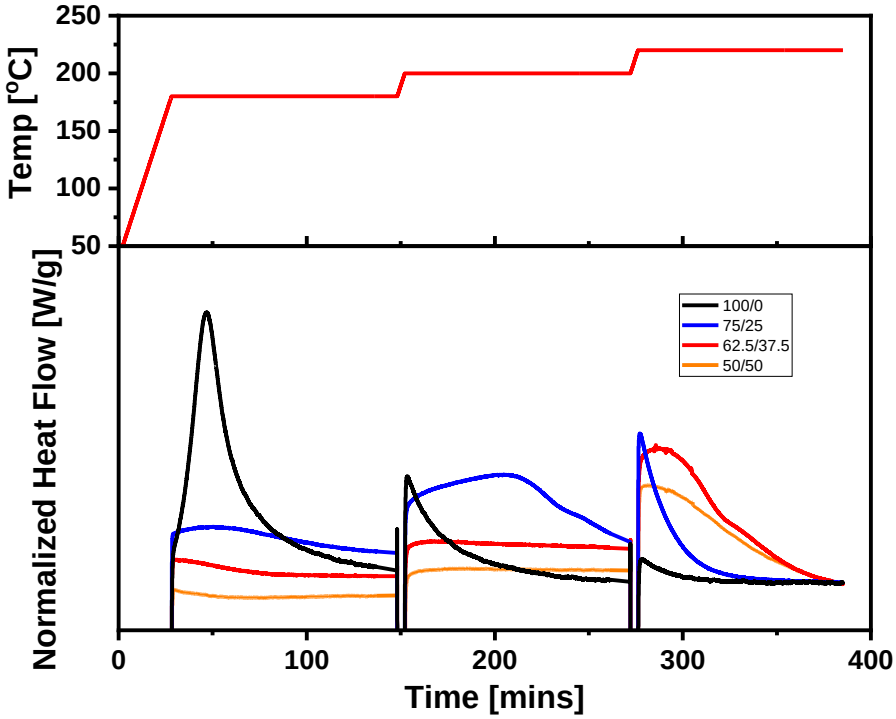

Figure 35: Bz/TGAP blends under known Bz and Bz/CER cure profile.

The lack of exothermic activity below 220 °C suggests that the cure profile is not suitable for the TGAP blends, and that the Bz and TGAP have not fully reacted and formed a crosslinked structure.

TGA was performed on several of the TGAP blends, as well as the pure monomers to observe their initial degradation temperature. A temperature ramp from 30 °C – 900 °C was implemented at 5 °C/min. A 5-7% weight loss is observed for Bz monomers as well as the blends at ~260 °C. The TGAP monomer exhibits 80% weight loss, from 250 °C to 300 °C. TGAP weight loss is noticeably reduced upon introduction of Bz into the blend. Weight loss at 300 °C drops from 80% for the neat TGAP, to ~8-12% depending on the amount of Bz in the blend.

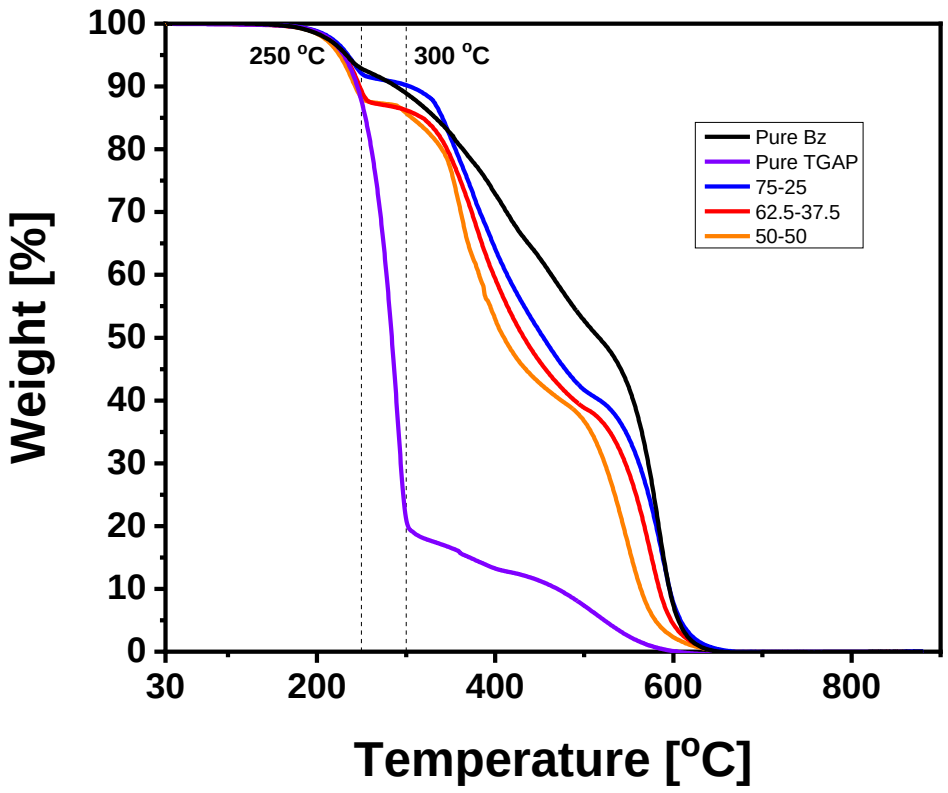

Figure 36: TGA of uncured monomers and TGAP blends.

Given the two observations above, a DSC profile was run to observe where the exothermic cure activity of the blend ended. Four 2-hour isotherms were implemented at [220 °C, 240 °C, 260 °C and 280 °C] to simulate curing. The stoichiometric equivalent system was used for cure-profile identification to limit the number of contributing factors. The results are shown in Figure 37.

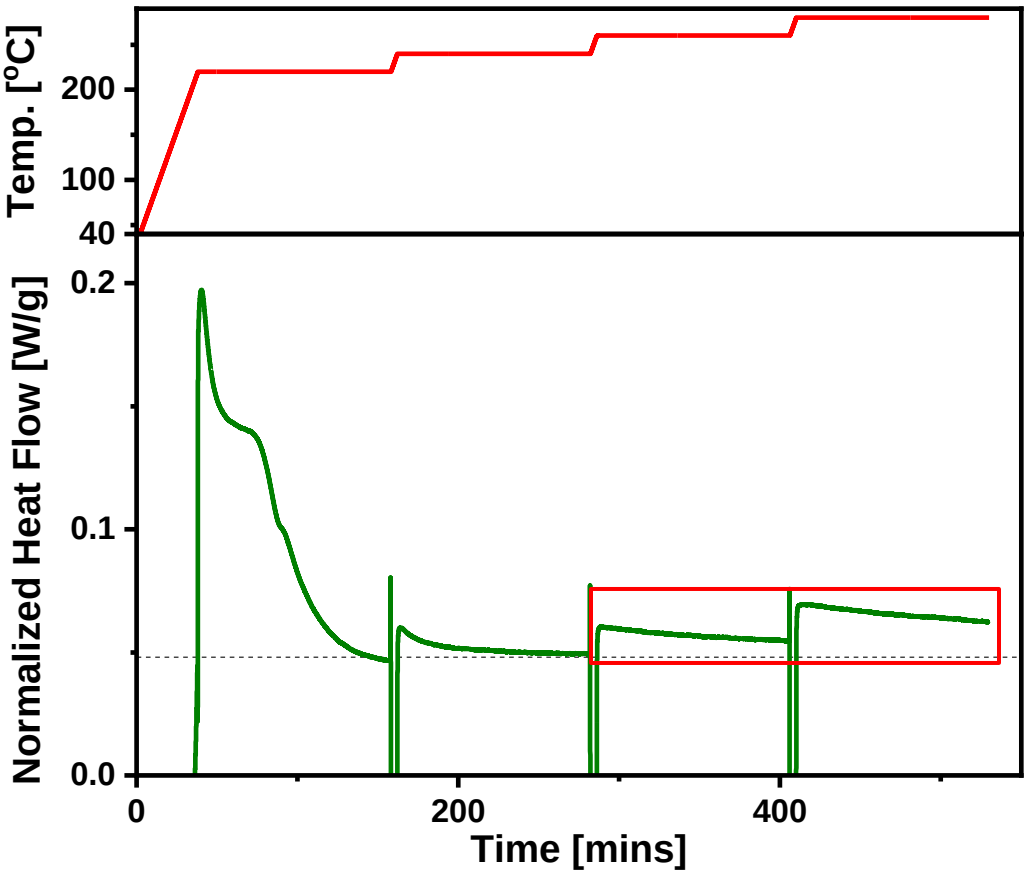

Figure 37: Elevated temperature cure profile to identify baseline and degradation.

A large exothermic event can be observed in Figure 37 during the first 2-hour isotherm at 220°C, followed by a smaller but significant exotherm at the second 2-hour isotherm at 240 °C. One important observation is that no activity is seen by the end of the 240 °C isotherm, signifying completion of cure.

5.2 DSC Characterization

5.2.1 Glass Transition Temperature

Bz-TGAP samples were made at weight percent concentrations (BZ/TGAP) of 100/0 (neat), 75/25, 70.4/29.6 (stoichiometric,) 62.5/37.5, 50/50 and 25/75 (epoxy rich blend). Figure 38 illustrates the DSC temperature sweeps used to identify the T_g of each blend.

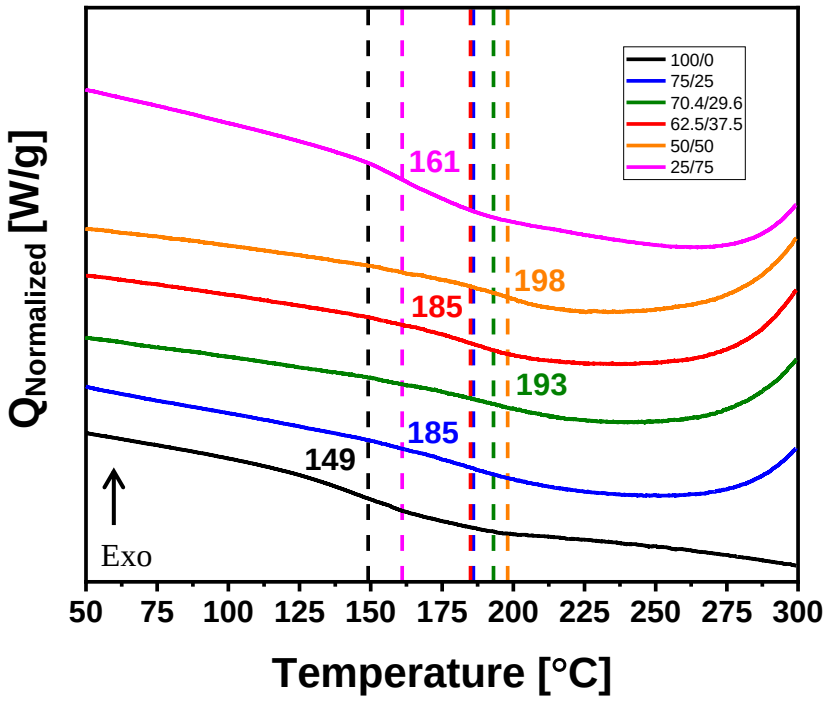

Figure 38: T_g sweeps for neat Bz and Bz/TGAP Blends.

Table 8: Glass transition as a function of TGAP wt. %.

Composition (Bz/Ep) [wt.%]	T_g [°C]
100/0	149
75/25	185
70.4/29.6	193
62.5/37.5	185
50/50	198
25/75	161

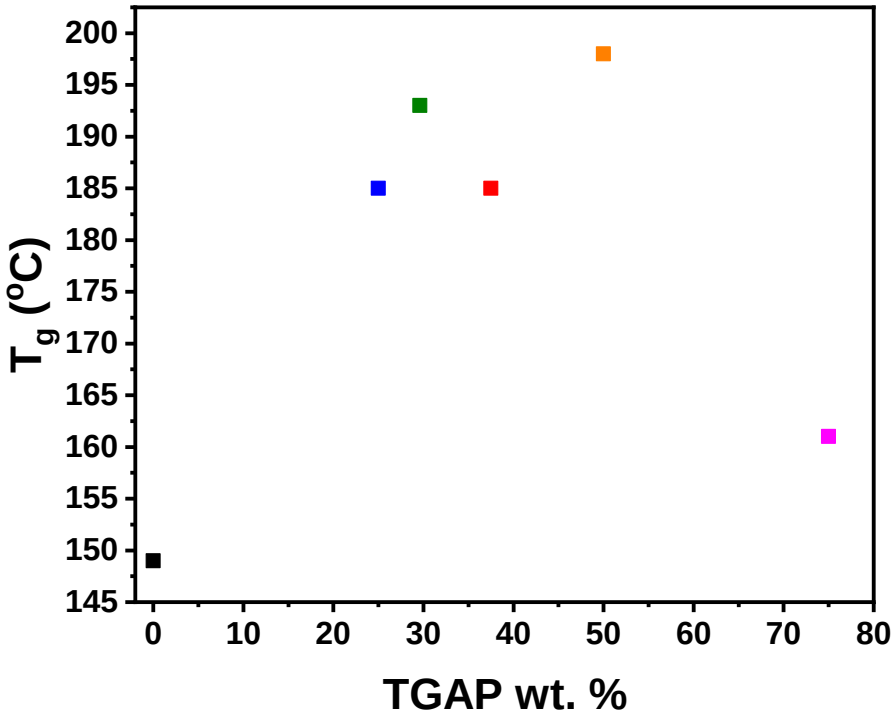

Figure 39: T_g vs. TGAP wt. %.

Figure 39 and Table 8 show the T_g's obtained from DSC of various weight percent blends**.** Most of the T_g's are above 180 °C and less dependent on epoxy weight percentage than the CER blends. The 50/50 composition exhibited the highest glass transition of 198 °C, with the stoichiometric blend falling only 5 °C below at 193 °C. The severely lowered T_g of the 25/75 blend likely originates from plasticization of the blend due to a large imbalance in reactive sites between the epoxy and the Bz. This will leave small chain length unreacted oligomers within the system. It should be mentioned that when TGAP is cured with a common curing agent such as diamino diphenyl sulfone, T_g values in the range of 176 °C can be obtained [44].

5.2.2 Heat of Reaction

Heat of reaction was calculated for each blend by subjecting an uncured resin sample to the predefined cure cycle on the DSC. For the Bz-TGAP blends, the cure profile consists of the following: 5 ^{o}C/min ramp to 220 ^{o}C, 2 hr isotherm at 220 ^{o}C, 5 /min ramp to 240 ^{o}C, 2 hr isotherm at 240 ^{o}C. The total heat of reaction is calculated by integrating the area under the curves during the three isothermal holds. Figure 40 displays the cure profile and resulting normalized heat flow obtained from the DSC for each composition. Table 10 and Figure 42 contain the calculated activation energies for each blend composition. Similar to the CER, the curing reaction is hindered by the addition of epoxy. Additionally, two exothermic peaks can be observed in blends containing more than 25 wt% epoxy, suggesting that there are two competing reactions that proceed during cure.

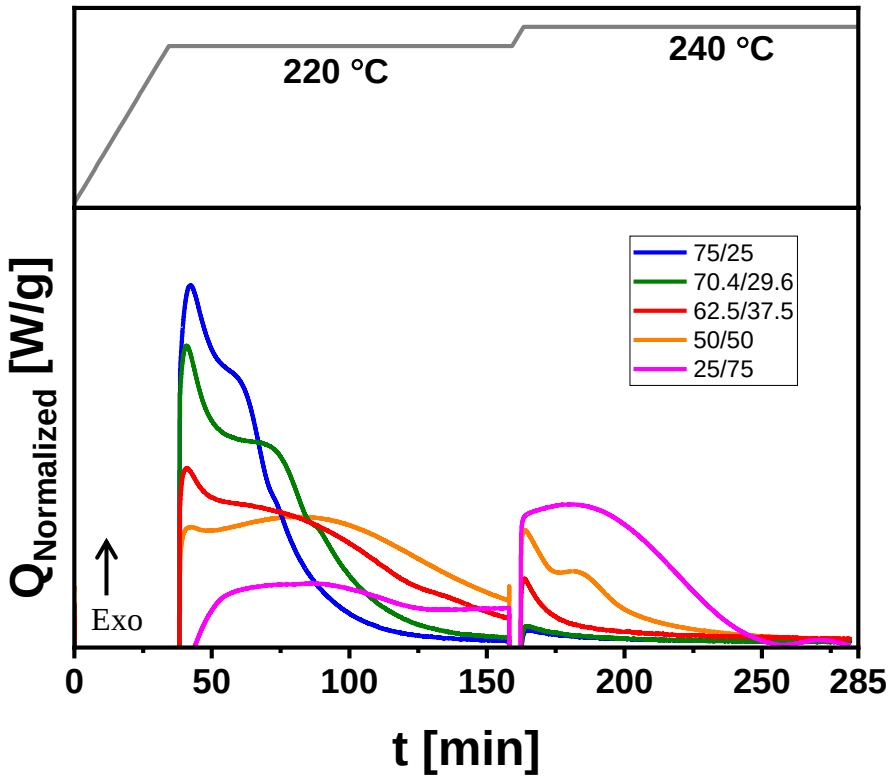

Figure 40: DSC Temperature sweep over defined TGAP cure profile.

Table 9: Heat of Reaction for Neat Bz and Bz/TGAP Blends.

Composition (Bz/EP) [wt%]	ΔH [J/g]
100/0	337
75/25	390
70.4/29.6	399
62.5/37.5	405
50/50	499
25/75	452

5.2.3 Degree of Conversion

Figure 41 shows the level of conversion that occurs at each isotherm. As a reminder, all trends are normalized to their respective heats of reaction and should not be taken as degree of cure. The purpose of Figure 41 is to show relative rates of cure throughout the two, two hour isotherms. As the wt% epoxy increases, the degree of conversion decreases drastically during the first isotherm.

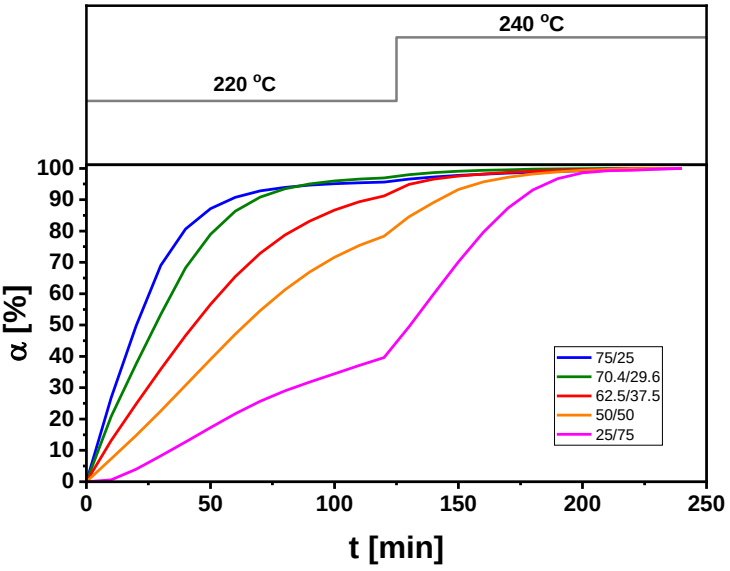

Figure 41: Degree of Conversion for Neat Bz and Bz/TGAP Blends.

5.2.4 Activation Energy: Kissinger Method

Figure 42 shows the Kissinger relation for each blend at [1, 2, 5, 10, 20] ^{o}C/min and the resulting activation energy reported in Table 10.

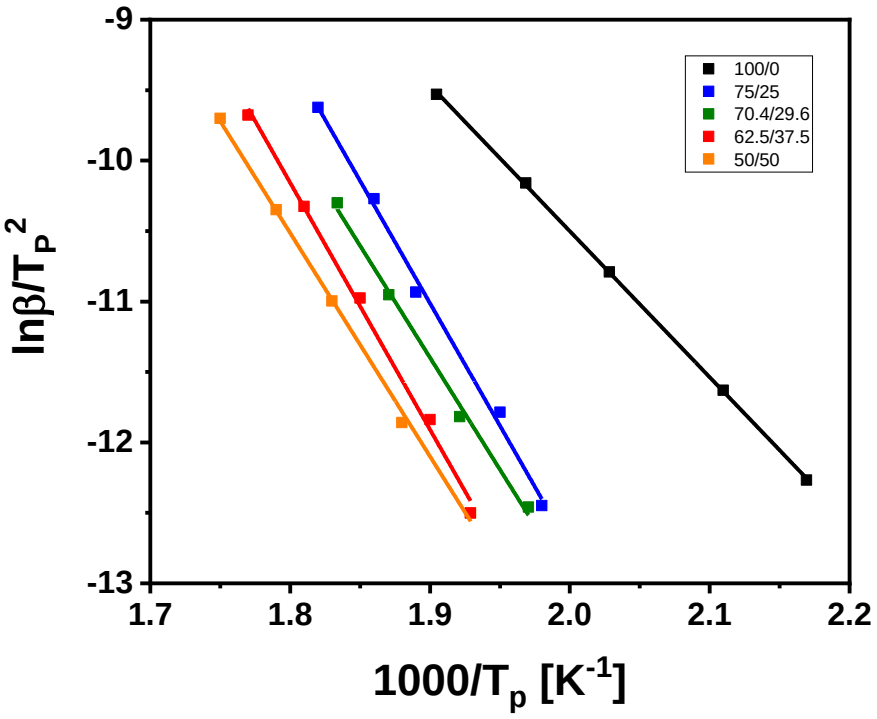

Figure 42: Kissinger method plots for Activation Energy of Neat Bz and Bz/TGAP Blends.

Table 10: Calculated Activation Energy for neat Bz and Bz/TGAP Blends.

Composition (Bz/TGAP) [wt.%]	Activation Energy [kJ/mol]
100/0	86.1
75/25	144.4
70.4/29.6	132.1
62.5/37.5	145.6
50/50	131.8

Activation energy increases by ~53-69% upon the addition TGAP into the system. The highest activation energy is reported for the 62.5/37.5 composition, however, these

runs were not reproduced, so it is likely that all systems with TGAP added are within error of each other. The drastic increase in activation energies is due to the non-linear nature of the monomer. The more sterically hindered the network becomes, the more energy is required to form crosslinks. This behavior is unlike that observed in the di-functional Bz/CER system, where little no increase in activation energy was observed upon the addition of epoxy.

5.3 DMA Characterization

Pre-mixed blends were preheated to 130 ^{o}C and poured into molds for torsional sample preparation. Samples were degassed at 130 ^{o}C for 20-30 min until no bubbles were visible. Cure profiles for the neat Bz-a and Bz/Ep are shown in Figure 13. Samples were tested for T_g's and crosslink densities calculated from the rubbery plateau modulus, more specifically at T_g + 50. Torsional DMA measurements were performed with a strain amplitude of 0.05%, a frequency of 1 Hz and with a temperature ramp from 30-300 ^{o}C at 5 ^{o}C/min. Tan(δ) for each blend is shown in Figure 43 and accompanying T_g's in Figure 44 and Table 11.

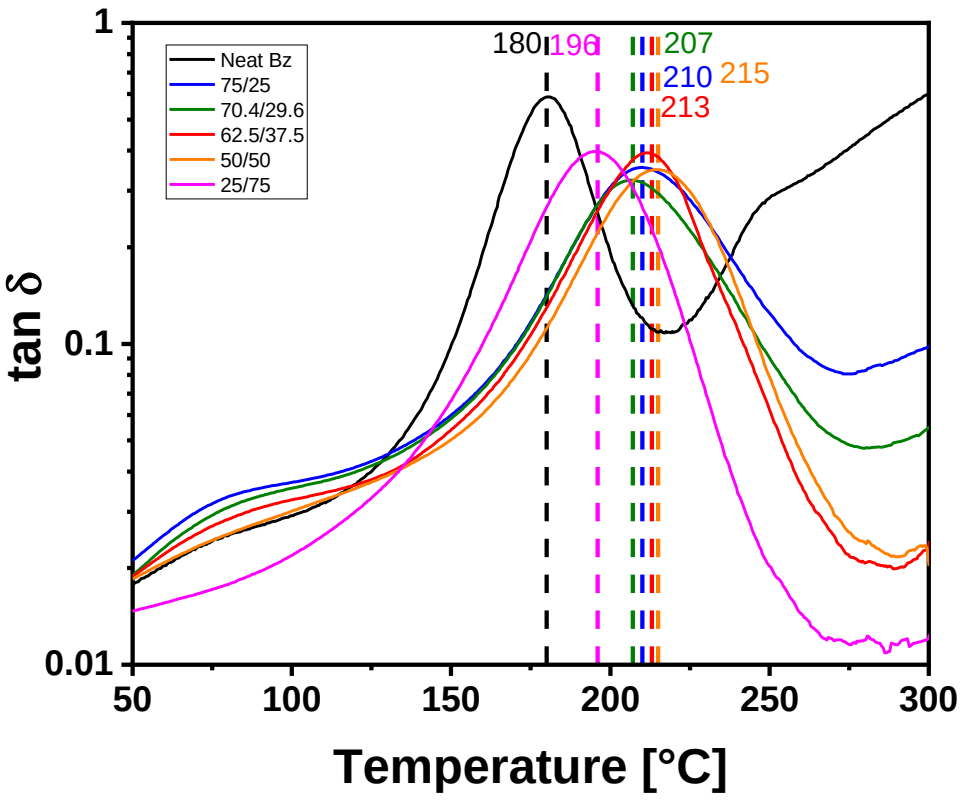

Figure 43: DMA Temperature sweeps for glass transition of neat Bz and Bz/TGAP blends.

Table 11: Tg via DMA.

Composition (Bz/TGAP) [wt%]	**T_g [°C]**
100/0	180
75/25	210
70.4/29.6	207
62.5/37.5	213
50/50	215
25/75	196

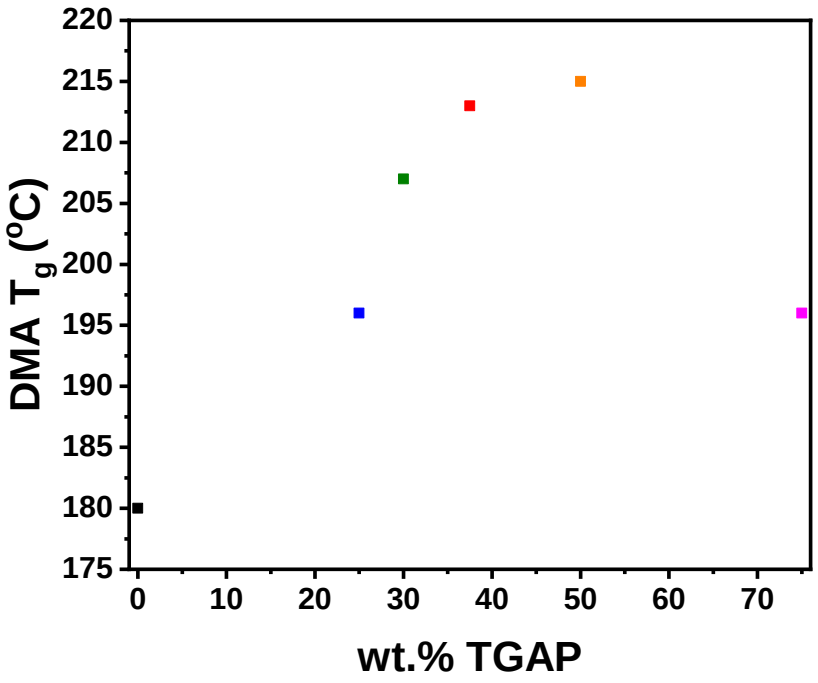

Figure 44: T_g vs. wt. % TGAP via DMA.

The T_g's of the blends increase with increasing wt.% of epoxy. There is roughly a 35 °C temperature gap between the neat Bz-a and the 50/50 Bz/TGAP blend. Unlike the CER blends, the TGAP blends exhibit somewhat of a plateau in resulting T_g's after 25 wt% TGAP is added.

Storage and loss modulus curves via torsion are shown in Figure 45, values at 35 °C are shown in Table 12. Equation 1 describes how crosslink density is calculated.

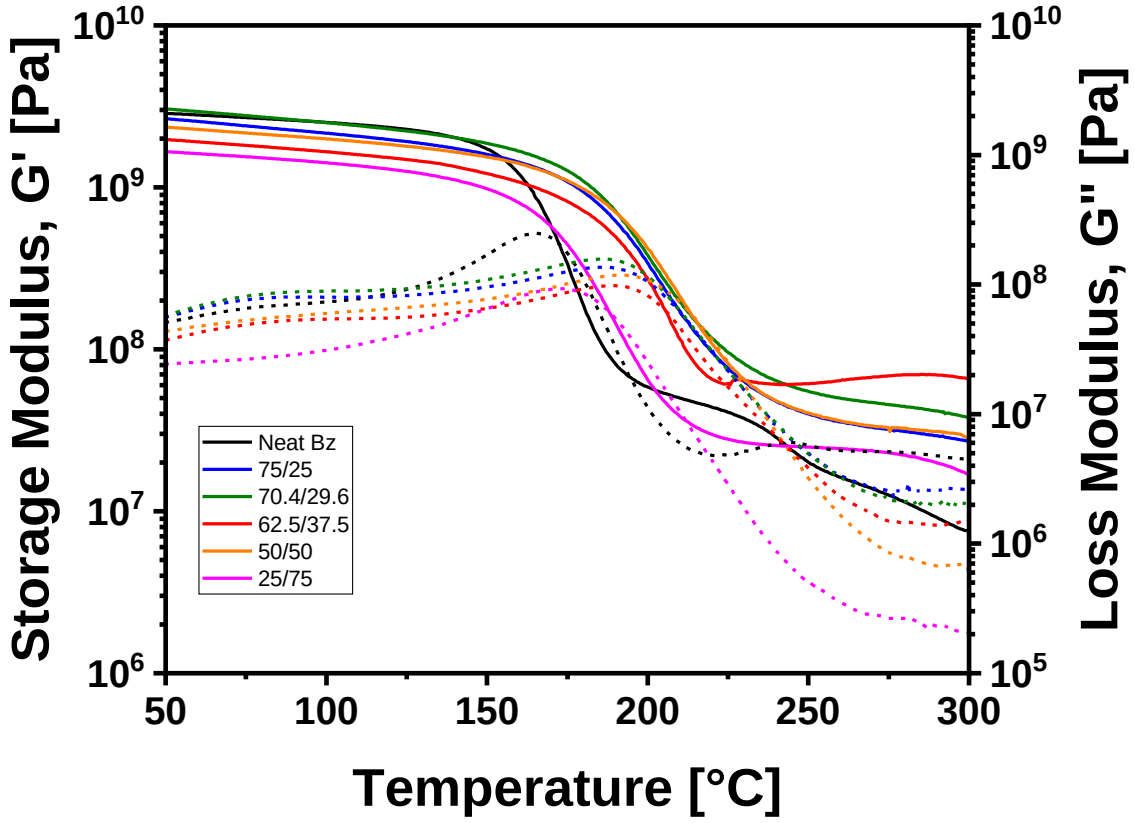

Figure 45: Temperature sweeps for Storage Modulus and Loss Modulus of Neat Bz and Bz/TGAP Blends.

Table 12: Storage Modulus, Loss Modulus and Crosslink Density of Neat Bz and Bz/CER Blends.

Composition [Bz/Ep wt%]	G'(35 °C) [GPa]	G"(35 °C) [MPa]	ν [mol/m^3]
100/0	3.0	42.8	2750
75/25	2.8	45.5	8034
70.4/29.6	3.2	46.9	11579
62.5/37.5	2.1	31.0	14698
50/50	2.5	39.3	7735
25/75	1.7	23.8	5794

Modulus appears to decrease upon the initial addition of TGAP into the system. The stoichiometric blend exhibits a modulus slightly above that of the neat Bz. The modulus of the 25/75 blend is significantly lower than that of the neat Bz or any of the other blends, this is in line with the results from calculating heats of enthalpy and can possibly be explained by the hindering of the cure reaction due to a severe imbalance of reactive sites. Given the blend is so far from its stoichiometric equivalent, the final cured product may exhibit pockets or nodules of heterogeneity that detrimentally affect mechanical properties. Crosslink density follows a similar trend as modulus, excluding the 62.5/37.5 blend crosslink density.

5.4 Tensile Characterization

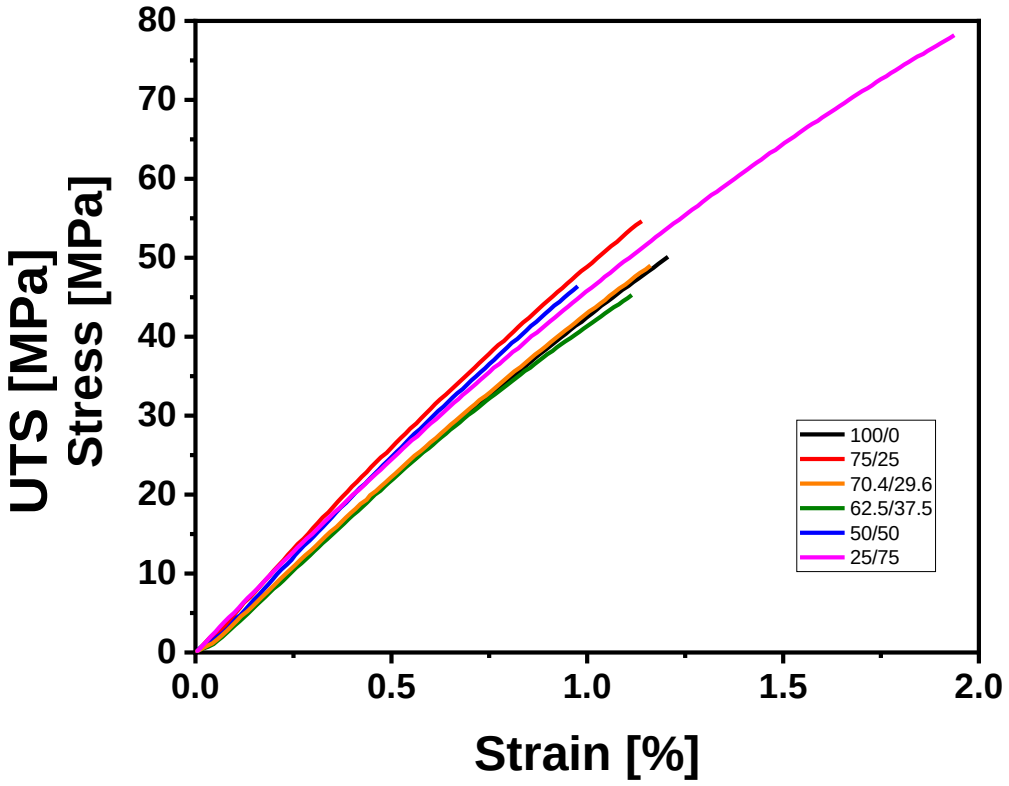

Figure 46: Representative Stress-strain curves for neat Bz and Bz/TGAP Blends.

Table 13: Average Stress, Strain and Modulus for neat Bz and Bz/TGAP Blends.

wt. % TGAP	Modulus [GPa]	UTS [MPa]	Strain at Failure [%]
100/0	4.1 ± 0.1	52.3 ± 11	1.4 ± 0.5
75/25	5.1 ± 0.3	45.0 ± 12	1.0 ± 0.3
70.4/29.6	5.2 ± 0.4	50.1 ± 6	1.1 ± 0.2
62.5/37.5	5.2 ± 0.3	56.0 ± 9	1.2 ± 0.2
50/50	4.5 ± 0.3	49.9 ± 10	1.2 ± 0.3
25/75	4.9 ± 0.3	78.2 ± 5	1.9 ± 0.2

Tensile strength of neat benzoxazine was found to be 52.3 ± 11 MPa with little to no change with added TGAP excluding the 25/75 composition. Tensile strength of the 25/75 composition was reported to increase by ~50%, all other blend tensile strengths are within error of each other.

Strain to failure for neat Bz was 1.4 ± 0.5 % and decreased to a minimum value at 75 wt.% TGAP of 1.0 ± 0.3 %. The 25/75 blend exhibited a notable increase of 36% in strain to failure, with all other samples exhibiting strain to failure nearly within error of the neat benzoxazine

Tensile modulus of neat Bz was measured to be 4.13 ± 0.09 GPa and increased 26% to 5.21 ± 0.39 when the stoichiometric equivalent system was characterized. Beyond 37.5 wt.% TGAP, the moduli only increased ~10-18% for 50/50 and 25/75 compositions.

5.5 FT-IR Characterization

Figure 47 depicts FTIR of uncured monomers. The uncured TGAP exhibits 4 strong characteristic peaks. Stretching of the epoxide group can be seen at 905 cm^{-1}, CH stretch within the range of 2665-3150 cm^{-1}, para-benzene stretch at 1514 cm^{-1}, and a tertiary amine stretch at 1297 cm^{-1}. It is worth noting that the epoxide peak location for the TGAP is

slightly different than the CER due to the chemical structure of the monomers. The CER epoxide peak is located at 945 cm^{-1} while the TGAP epoxide peak is located at 905 cm^{-1} These peaks are observed throughout the cure, however, their relative intensities are found to decrease by the end of the implemented cure cycle.

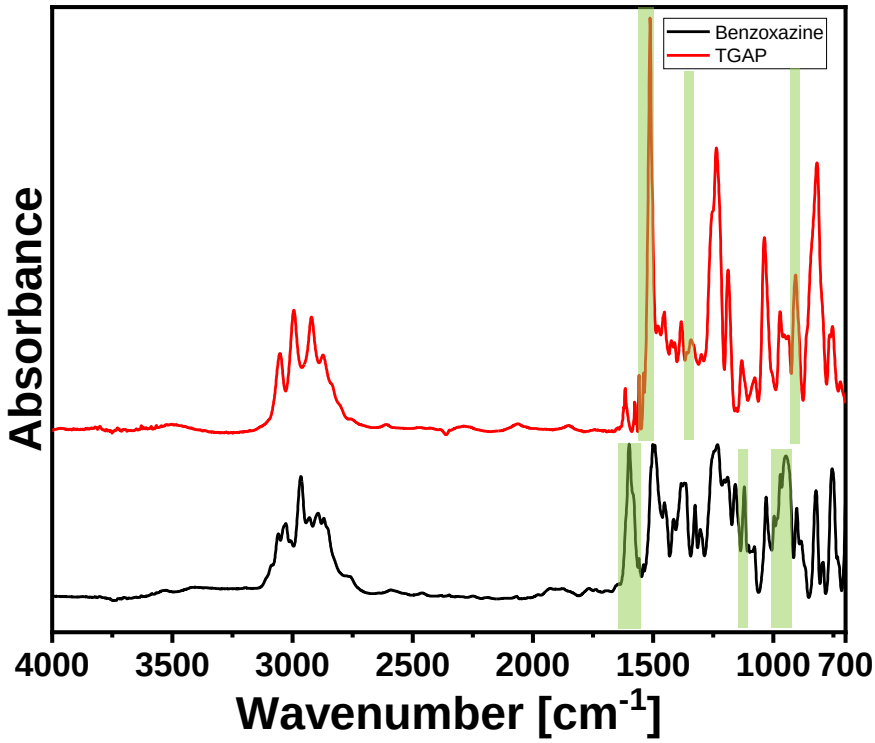

Figure 47: Monomer FTIR, Bz and TGAP.

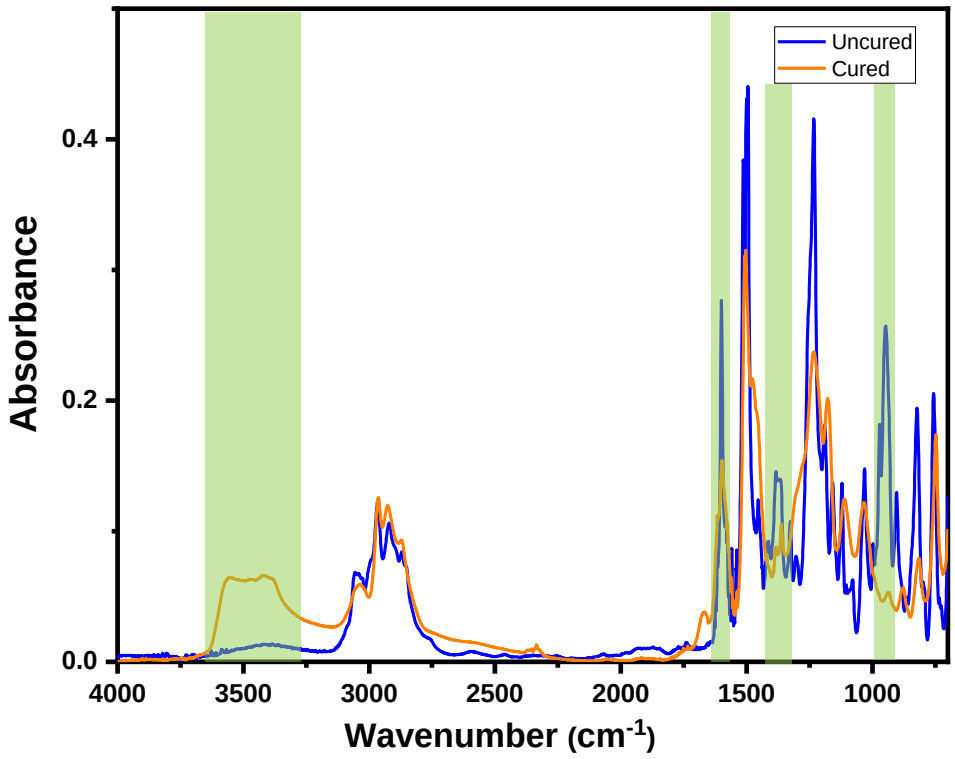

Figure 48: First and last spectra from in-situ FTIR of Bz/TGAP stoichiometric blend.

First and last spectra from in situ FT-IR of the stoichiometrically balanced Bz/TGAP blend is shown in Figure 48. The hybrid network is formed initially through the ring opening polymerization of the Bz. As OH sites become available via the opening of the oxazine ring, the epoxide groups from the TGAP can readily crosslink into the network. The proposed mechanism is shown previously in Figure 34.

The FT-IR spectra of the blend in Figure 48 shares peaks from the scans of the TGAP and Bz monomers. The consumption of the oxazine ring is seen at 945 cm^{-1}. The N-C-O stretch located at 1600 cm^{-1} is also visible and decreases in absorbance as cure proceeds, signifying crosslink formation with other Bz monomers or epoxide groups of the TGAP monomers. Peaks that are unique to the TGAP include: Para-benzene stretch at 1514 cm^{-1}, tertiary amine stretch at 1297 cm^{-1} and an epoxide stretch at 905 cm^{-1}. Peaks from the

Bz monomer can also be observed at 945 cm^{-1} (oxazine ring) and 1600 cm^{-1} N-C-O stretch. The epoxide, oxazine ring and N-C-O stretch peaks all decrease in absorbance throughout progression of cure, signifying a hybrid network formation. Product peaks include Intermolecular OH-O hydrogen bonding at wavenumber 3375 cm^{-1} and intramolecular OH-π hydrogen bonding at 3540 cm^{-1} [29].

5.5 Summary and Conclusions

All of the Bz/TGAP blends exhibited an increase in T_g via DSC and DMA upon addition of CER. The 50/50 blend exhibited the highest T_g of 215 ^oC, followed closely by the 62.5/37.5 blend at 213 ^oC and the stoichiometric equivalent blend at 207 ^oC. Crosslink density was found to increase from 2750 mol/m^3 in neat Bz to a maximum of 14698 mol/m^3 in the 62.5/37.5 blend.

Unlike the Bz/CER based system, there is a significant increase of ~53-69% in activation energy upon addition of TGAP. None of the Bz/TGAP tan(δ) curves exhibit broadening, signifying that each composition was homogenously crosslinked.

When tensile testing results are considered, the stoichiometric equivalent Bz/TGAP exhibits a desirable combination of modulus and ultimate tensile strength. Given the 25/75 only experiences a 16 ^oC increase in T_g relative to the neat Bz, this composition can be ruled out of selection for the most optimal composition. Considering the combination of high thermal and mechanical properties exhibited by the stoichiometric equivalent composition, this composition should be selected as the most optimal blend composition for use in applications.

CHAPTER 6

CONCLUSIONS AND FUTURE WORK

6.1 Conclusion

Thermo-mechanical properties and cure kinetics were investigated for a neat Bz system as well as binary systems of Bz-CER and Bz-TGAP. Compositions by wt% investigated include: 100/0, 75/25, stoichiometric (63.8/26.2 for CER, 70.4/29.6 for TGAP), 62.5/37.5, 50/50 and 25/75. T_g was measured via DSC and DMA, revealing an interesting synergistic increase in T_g upon blending both types of epoxy with Bz. DSC thermograms reveal a single exothermic peak in the neat Bz system, as well as in all the Bz/CER systems up to 50/50 wt%. At and above 50/50 wt. % in the Bz/CER system, two exothermic peaks during a single isotherm are visible, and peak broadening occurs in the tan(δ) signifying a distribution of relaxation times and a heterogenous network of crosslinks. This type of behavior is undesirable and should remove the 50/50 Bz/CER blend from consideration as an optimal blend composition.

T_g of the neat Bz via DMA was reported to be 180^{o}C. The maximum reported T_g for Bz/CER systems via DMA was 245 ^{o}C for the 50/50 composition, followed closely by the stoichiometric equivalent at 243 ^{o}C and the 62.5/37.5 composition at 242 ^{o}C. In the TGAP systems, two exothermic peaks can be observed for each composition investigated. The maximum reported T_g via DMA for the Bz/TGAP system was achieved in the 50/50 composition, followed closely by the 62.5/37.5 composition at 213 ^{o}C and the stoichiometric equivalent composition at 207 ^{o}C. The T_g measurements taken for the Bz/CER system follow the results published by Barjasteh et. al. closely [14].

Heat of reaction was found by integrating the normalized heat flow over the duration of the defined cure profile for each system. The heat of reaction for neat Bz is 337 J/g. Heat of reaction for the Bz/CER system increased to a maximum of 405 J/g upon addition of 25 wt.% epoxy and decreased to a minimum of 75 J/g when 75 wt.% CER was added. Heat of reaction for the Bz/TGAP system increased to a maximum of 499 J/g at 50 wt.% TGAP, dropping slightly to 452 J/g when 75 wt.% TGAP was added.

Activation energies were calculated using the Kissinger method for all compositions. Blends containing CER exhibited an increase in activation energy of ~ 12 % for compositions below 50 wt.% CER. At 50 wt.% CER the activation energy was reported to increase 24 %. These results match closely with the work reported by Barjasteh et. al. Blends containing TGAP exhibited an increase in activation energy up with addition of up to 50 wt. % epoxy. A maximum heat of reaction of 499 J/g is achieved in the 50/50 composition, dropping slightly to 452 J/g when 75 wt. % TGAP was added.

Crosslink density values for the neat system and blended systems were calculated using modulus values obtained from T_g + 50. Neat Bz was reported to have a crosslink density of 2750 mol/m^3. Crosslink density increased by nearly 300% to a maximum of 10237 mol/m^3 in the 25/75 composition. The consistent increase in crosslink density corroborates the trend found by Barjasteh et. al., however, the values reported here are slightly higher at each composition. Crosslink density increased by over 400% to a maximum of 14698 mol/m^3 in the 62.5/37.5 Bz/TGAP system. The significant increase in crosslink density can be explained by the introduction of additional crosslinking sites located on the oxirane groups of both epoxy monomers. The substantial difference in T_g

between the neat system and the blended systems can partially be explained by the dramatic increase of crosslink density.

In-situ FT-IR scans of each system reveal the opening of the oxazine ring at the N-C-O bond location. Absorbance at wavenumbers representative of oxazine ring stretch, N-C-O stretch and oxirane stretch were found to decrease throughout cure for all the systems. Product peaks were observed within the range 3300-3540 cm^{-1} representative of intermolecular and intramolecular hydrogen bonding. Hydrogen bonding contributes to the increased T_g observed in the hybrid network polymerized Bz/CER and Bz/TGAP systems [30]. Hydrogen bonding also occurs in the neat Bz system, however, the number of available sites for hydrogen bonding greatly increases with the introduction of an epoxy monomer.

Tensile tests were performed on each blend composition. The neat Bz system exhibited a modulus of 4.13 ±0.09 GPa, an ultimate tensile strength of 52.3 ±11 MPa and 1.4 ± 0.5 % strain at break. In the case of the CER system, the 75/25 composition displayed the highest modulus value of 4.97 ±0.09 GPa, an ultimate tensile strength of 49.2 MPa and 1.1% strain at break. These tensile results are consistently higher than those reported by Barjasteh et. al. [14] and Ishida [15], and no significant decrease in modulus is observed with addition of CER. For the TGAP system, the 62.5/37.5 composition displayed the highest modulus of 5.22 ± 0.27 GPa, an ultimate tensile strength of 56 ± 9 MPa and a strain at break of 1.2 ± 0.2. These results partially agree with those published by Ishida [15] and Barjasteh[14].

6.2 Future Work

The work of this thesis explores the optimal blending conditions for two systems, Bz/CER and Bz/TGAP. The effect of functionality of blended epoxy is also explored. FT-IR characterization of the blends pre- and post-cure were performed, but only qualitative remarks were made. Moving forward, a more thorough analysis of *in-situ* FT-IR data of each system should be performed. Concentration profiles can be mapped with proper calculation of molar absorptivity coefficients as well as accurate baselining and background correction of the collected raw data. Peak heights and areas must also be tracked throughout the cure, and peaks deconvoluted in each file. This work lies outside of the scope of this thesis and requires more extensive knowledge of both Matlab and FT-IR data analysis.

Incorporation of filler and the effects on final macro-scale thermo-mechanical properties should be investigated. Given the inherent brittle nature of the neat Bz, blended Bz/CER and Bz/TGAP systems, toughening of the systems would be of interest. Rubber particles could be incorporated to improve toughness of the matrix. Additionally, rubber with various terminal functional groups could also be explored. Implementing rubber with functional groups capable of crosslinking into the network could improve the overall toughness of the system. Rubber with functional groups capable of forming hydrogen bonds with the network should also be explored.

APPENDIX A

FT-IR of Off-Stoichiometric Bz/CER and Bz/TGAP Blends

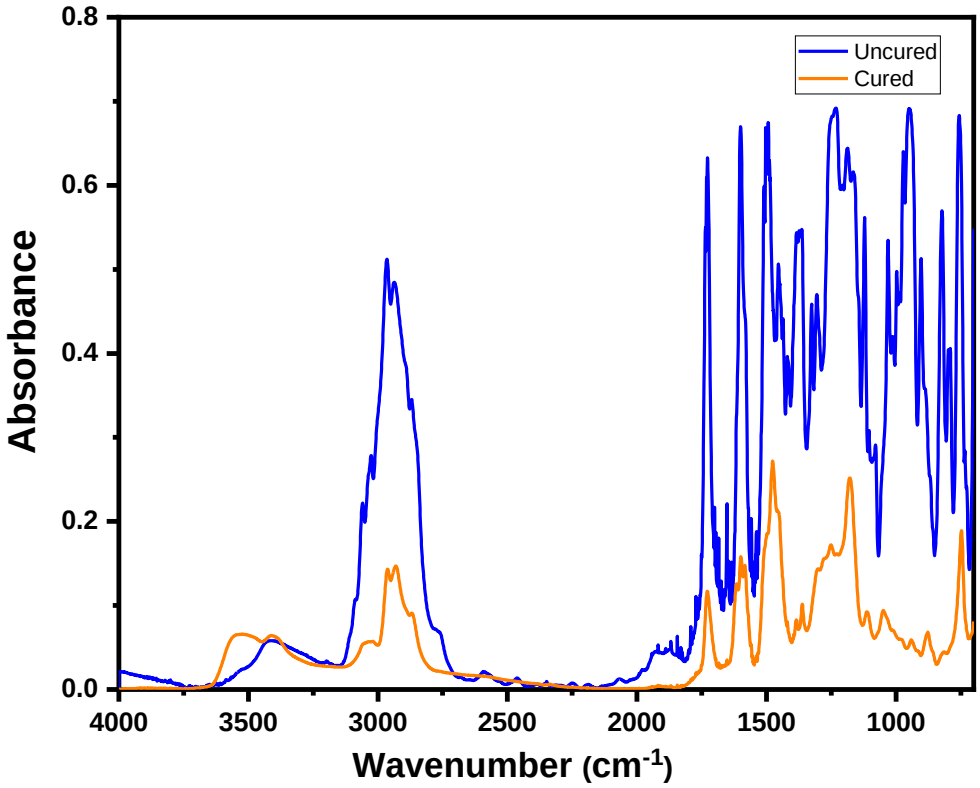

Figure 49: First-Last FTIR 50/50 Bz/CER Epoxy.

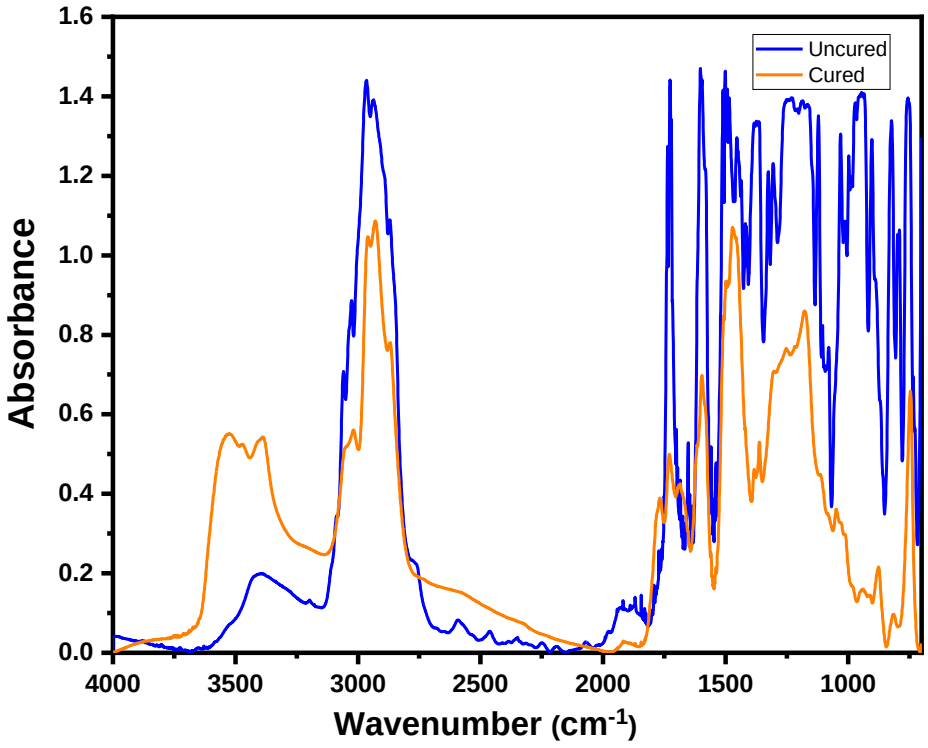

Figure 50: First-Last FTIR 75/25 Bz/TGAP.

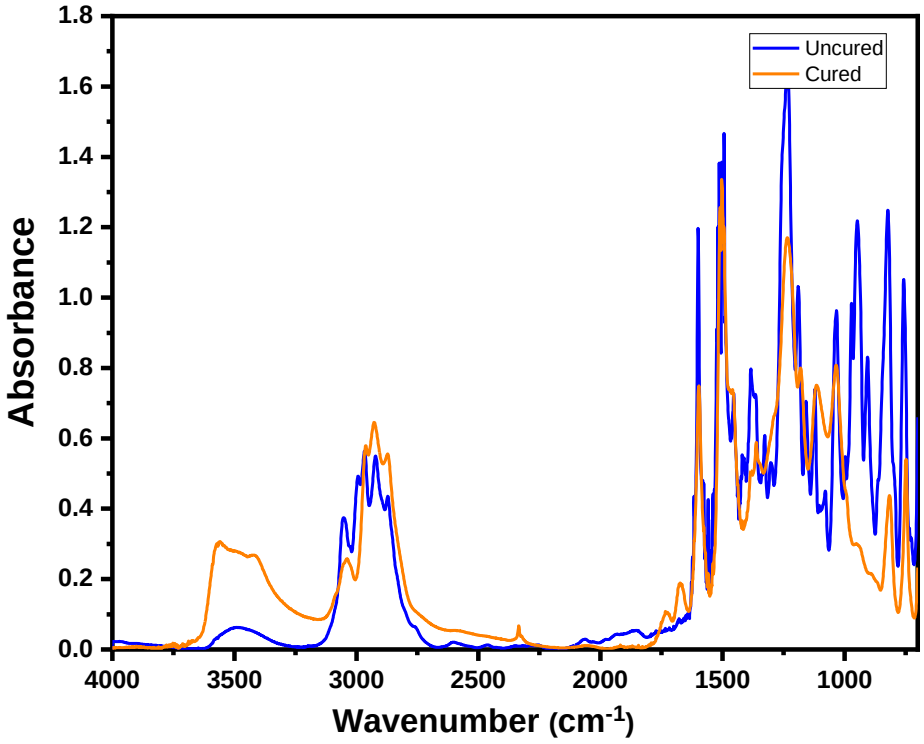

Figure 51: First-Last FTIR 50/50 Bz/TGAP.

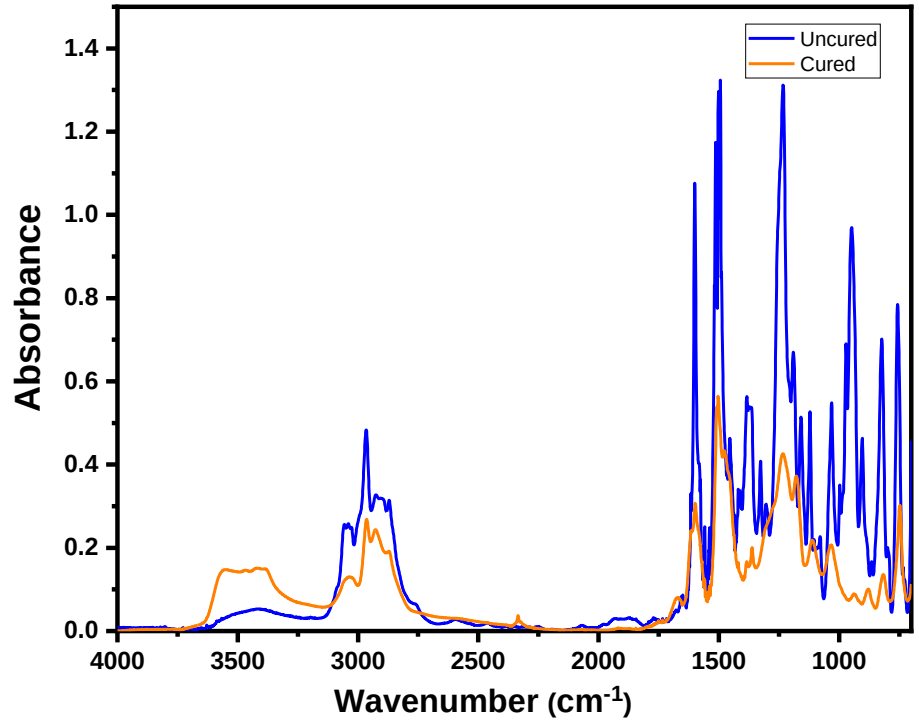

Figure 52: First-Last FTIR 75/25 Bz/TGAP.

REFERENCES

1. Dodiuk, H. and S.H. Goodman, *Handbook of Thermoset Plastics*. 2014: Elsevier.
2. Agag, T., T. Koga, and T. Takeichi, *Studies on thermal and mechanical properties of polyimide–clay nanocomposites.* Polymer, 2001. **42**(8): p. 3399-3408.
3. Rozenberg, B.A., et al., *High-performance bismaleimide matrices: cure kinetics and mechanism.* Polymers for Advanced Technologies, 2002. **13**(10-12): p. 837-844.
4. Wooster, T.J., et al., *Thermal, mechanical, and conductivity properties of cyanate ester composites.* Composites Part A: Applied Science and Manufacturing, 2004. **35**(1): p. 75-82.
5. Campbell, F.C., *Manufacturing Process for Advanced Composites*. 2004.
6. Ishida, H. and H.Y. Low, *A Study on the Volumetric Expansion of Benzoxazine-Based Phenolic Resin.* Macromolecules, 1997. **30**(4): p. 1099-1106.
7. Ishida, H. and T. Agag, *Handbook of Benzoxazine Resins*. 2011: Elseveir.
8. Ning, X. and H. Ishida, *Phenolic materials via ring-opening polymerization: Synthesis and characterization of bisphenol-A based benzoxazines and their polymers.* Journal of Polymer Science Part A: Polymer Chemistry, 1994. **32**(6): p. 1121-1129.
9. Kim, H.-D. and H. Ishida, *Study on the chemical stability of benzoxazine-based phenolic resins in carboxylic acids.* Journal of Applied Polymer Science, 2001. **79**(7): p. 1207-1219.

10. Ghosh, N.N., B. Kiskan, and Y. Yagci, *Polybenzoxazines—New high performance thermosetting resins: Synthesis and properties.* Progress in Polymer Science, 2007. **32**(11): p. 1344-1391.

11. Takeichi, T., T. Kano, and T. Agag, *Synthesis and thermal cure of high molecular weight polybenzoxazine precursors and the properties of the thermosets.* Polymer, 2005. **46**(26): p. 12172-12180.

12. Dunkers, J. and H. Ishida, *Reaction of benzoxazine based phenolic resins with strong and weak carboxylic acids and phenols as catalysts.* Journal of Polymer Science: Part A: Polymer Chemistry, 1999. **37**: p. 1913-1921.

13. Sloan, J. *Polybenzoxazine on the horizon?* 2016; Available from: https://www.compositesworld.com/blog/post/polybenzoxazine-on-the-horizon.

14. Barjasteh, E., et al., *Bisphenol-A benzoxazine and cycloaliphatic epoxy copolymer for composite processing by resin infusion.* Journal of Composite Materials, 2018. **53**(13): p. 1777-1790.

15. Ishida, H. and D. Allen J., *Mechanical Characterization of copolymers based on benzoxazine and epoxy.* Polymer, 1996. **37**(20): p. 4487-4495.

16. Ishida, H. and D. Allen J., *Physical and Mechanical Characterization of Near-Zero Shrinkage Polybenzoxazines.* Journal of Polymer Science Part B: Polymer Physics, 1996. **34**: p. 1019-1030.

17. Han, L., et al., *Study of the Effects of Intramolecular and Intermolecular Hydrogen-Bonding Systems on the Polymerization of Amide-Containing Benzoxazines.* Macromolecular Chemistry and Physics, 2017. **218**(18): p. 1600562.

18. Rimdusit, S., P. Kunopast, and I. Dueramae, *Thermomechanical properties of arylamine-based benzoxazine resins alloyed with epoxy resin.* Polymer Engineering & Science, 2011. **51**(9): p. 1797-1807.

19. Rimdusit, S., et al., *Toughening of polybenzoxazine by alloying with urethane prepolymer and flexible epoxy: A comparative study.* Polymer Engineering & Science, 2005. **45**(3): p. 288-296.

20. Santhosh Kumar, K.S. and C.P. Reghunadhan Nair, *Polybenzoxazine–new generation phenolics.* 2014: p. 45-73.

21. Yousefi, A., P.G. Lafleur, and R. Gauvin, *Kinetic studies of thermoset cure reactions: A review.* Polymer Composites, 1997. **18**(2): p. 157-168.

22. Urbaniak, M. and K. Grudziński, *Time-temperature-transformation (TTT) cure diagram for EPY® epoxy system.* Polimery -Warsaw-, 2007. **52**: p. 117-126.

23. Vyazovkin, S. and N. Sbirrazzuoli, *Isoconversional Kinetic Analysis of Thermally Stimulated Processes in Polymers.* Macromolecular Rapid Communications, 2006. **27**(18): p. 1515-1532.

24. Sabzevari, S.M., *Cure kinetics and process modeling of a carbon-fiber thermoplastic-toughened epoxy resin prepreg*, in *Mechanical Engineering*. 2010, Wichita State University. p. 118.

25. Liu, C. and Q.Y. Chen, *Advanced and Emerging polybenzoxazine science and technology*. 2017: Elsevier.

26. Gouni, S., *Cure Kinetics of Benzoxazine/Cycloaliphatic Epoxy Resin By Differential Scanning Calorimetry*, in *Materials Science*. 2018, California State University, Long Beach. p. 82.

27. Rimdusit, S. and H. Ishida, *Synergism and Multiple Mechanical Relaxations Observed in Ternary systems based on benzoxazine epoxy and phenolic resins.* Journal of Polymer Science Part B: Polymer Physics, 2000. **38**: p. 1687-1698.

28. Ishida, H. and S. Ohba, *Thermal analysis and mechanical characterization of maleimide-functionalized benzoxazine/epoxy copolymers.* Journal of Applied Polymer Science, 2006. **101**(3): p. 1670-1677.

29. Shen, X., et al., *How Does the Hydrogen Bonding Interaction Influence the Properties of Polybenzoxazine? An Experimental Study Combined with Computer Simulation.* Macromolecules, 2018. **51**(13): p. 4782-4799.

30. Huang, J.-M. and S.-J. Yang, *Studying the miscibility and thermal behavior of polybenzoxazine/poly(ε-caprolactone) blends using DSC, DMA, and solid state 13C NMR spectroscopy.* Polymer, 2005. **46**(19): p. 8068-8078.

31. Agag, T. and T. Takeichi, *Polybenzoxazine–montmorillonite hybrid nanocomposites: synthesis and characterization.* Polymer, 2000. **41**(19): p. 7083-7090.

32. Shen, S.B. and H. Ishida, *Development and characterization of high-performance polybenzoxazine composites.* Polymer Composites, 1996. **17**(5): p. 710-719.

33. Ishida, H. and Y.H. Lee, *Synergism observed in polybenzoxazine and poly(ε-caprolactone) blends by dynamic mechanical and thermogravimetric analysis.* Polymer, 2001. **42**(16): p. 6971-6979.

34. Jubsilp, C., T. Takeichi, and S. Rimdusit, *Effect of novel benzoxazine reactive diluent on processability and thermomechanical characteristics of bi-functional polybenzoxazine.* Journal of Applied Polymer Science, 2007. **104**(5): p. 2928-2938.

35. Lin, C.H., et al., *Flexible polybenzoxazine thermosets with high glass transition temperatures and low surface free energies.* Polymer Chemistry, 2012. **3**(4): p. 935-945.

36. Elmer, P., *Differential Scanning Calorimetry-A Beginners Guide*. 2013.

37. Leibniz-Institut. *Differential Scanning Calorimetry*. Available from: http://www.ipfdd.de.

38. Elmer, P., *Dynamic Mechanical Analysis - A Beginners Guide.* 2013.

39. Malek, J., *Kinetic analysis of crystallization processes in amorphous materials.* Thermochimica Acta, 2000. **335**: p. 239-253.

40. Kissinger, H., *Reaction Kinetics in Differntial Thermal Analysis.* Analytical Chemistry, 1957. **29**(11): p. 1702-1706.

41. Kultzow, R. and S. Foxhill, *Cycloaliphatic Epoxy Resins*. 2007, Huntsman Advanced Materials p. 6.

42. Gonzalez, M.G., J.C. Cabanelas, and J. Baselga, *Infrared Spectroscopy material science, engineering and technology*. 2012: InTech.

43. Zhang, K., et al., *Hydrogen-bonding characteristics and unique ring-opening polymerization behavior of Ortho-methylol functional benzoxazine.* Journal of Polymer Science Part A: Polymer Chemistry, 2016. **54**(22): p. 3635-3642.

44. Toledo, M., *Study of the curing behavior of a trifunctional epoxy*. 2014: Mettler toledo thermal analysis usercom 37. p. 5.